Economic Geology
Vol. 76, 1981, pp. 439–467

Geology and Genesis of the F-Sn-W(-Be-Zn) Skarn (Wrigglite) at Moina, Tasmania

T. A. P. KWAK

Department of Geology, La Trobe University, Bundoora, Victoria 3083, Australia

AND P. W. ASKINS*

Comalco Limited, Exploration Department, P. O. Box 691, Devonport, Tasmania 7310, Australia

Abstract

The Moina skarn deposit, with its associated Sn-W-F veins and greisen, occurs at the margin of the Dolcoath leucogranite. The skarn occurs as a thick horizontal plate approximately one km in its longest dimension and up to 100 m thick and is separated from the granite's upper near-horizontal contact by approximately 200 m of the Moina sandstone. The necessary plumbing system for access of mineralizing fluids is probably a series of east-west-trending tension fractures, now Sn-W quartz veins, associated with a major northwest-southeast-trending fault known as the Bismuth Creek fault. Emplacement of the granite was at shallow depths (<3 km?).

The skarn unit section consists of: (a) a granular garnet-pyroxene-vesuvianite-fluorite skarn; (b) the main skarn ("wrigglite") consisting of fluorite-magnetite-vesuvianite (cassiterite-scheelite-adularia) and having a characteristic fine-grained, rhythmic, finely layered contorted structure; (c) a granular, pale green pyroxene skarn which occurs as thin units (<5 cm) within and near the base of unit (b) above; (d) a wollastonite-rich skarn (>80 vol % wollastonite); and (e) a granular garnet-pyroxene-vesuvianite-fluorite skarn overlying the other units. Unit (e) is relatively enriched in boron (≃600 ppm).

The skarn unit carries up to 25 weight percent F; 0.6 percent Sn, 0.5 percent W, 0.2 percent Be, 27.5 percent Zn, and 4.5 ppm Au. Sn, Be, and Fe values increase toward the upper part of the skarn sequence whereas Zn, Cu, and Mo values are erratic. Secondary Zn-Cu-In-Cd-Au sulfide-amphibole alteration of the primary F-Sn-Be oxide skarn is related to the Bismuth Creek fault. When the primary wrigglite skarn is altered, Sn is largely lost from that part of the skarn.

Introduction

THE Moina skarn deposit is located 40 km southwest of Devonport, Tasmania, near the margin of the Devonian Dolcoath granite. Quartz lodes (veins) which cut the skarn and underlying quartzite were mined for Sn and W until 1956 (Jennings, 1965), but only recently has an investigation of the Fe-F-Sn-W-Be-Zn-Au skarns been reported (Askins, 1978). Apart from studies by Sainsbury (1964, 1969) and Jahns (1944a, b), little has been published on this type of skarn in the western literature, although much has been published in the USSR (e.g., Govorov, 1958, Getmanskaya, 1972; Miroshnchenko and Gulyayev, 1978).

In addition to being of obvious potential economic interest, the relationship of these Sn-bearing oxide skarns to Sn-bearing sulfide replacement deposits such as the Renison Bell deposit (Patterson, 1976) needs more study. The purpose of the present study has been to determine the mineralogy, paragenesis, and bulk chemical relationships of the skarn and related rocks; the nature of the mineralizing fluids; and the distribution of economic elements in the skarn. With this information, a genetic model has been suggested and relations to Sn-sulfide replacement deposits inferred.

* Present address: The Shell Company of Australia Ltd., William Street, Melbourne, Victoria 3000, Australia.

Geology, Petrology, and Mineralogy

General

At Moina F-Sn-W-Be(-Zn) mineralization occurs as skarn, in veins, and in greisen (Fig. 1A). The skarns are a replacement of essentially flat-lying Ordovician limestone and calcareous siltstone (the Gordon Limestone) which conformably overlies quartz sandstone and siltstone (the Moina sandstone).

Mineralization is associated with a Devonian leucocratic granite (Dolcoath granite) which is never in contact with the limestone or skarn but is separated by about 200 m of Moina sandstone. The most intense mineralization occurs in a folded and fractured zone

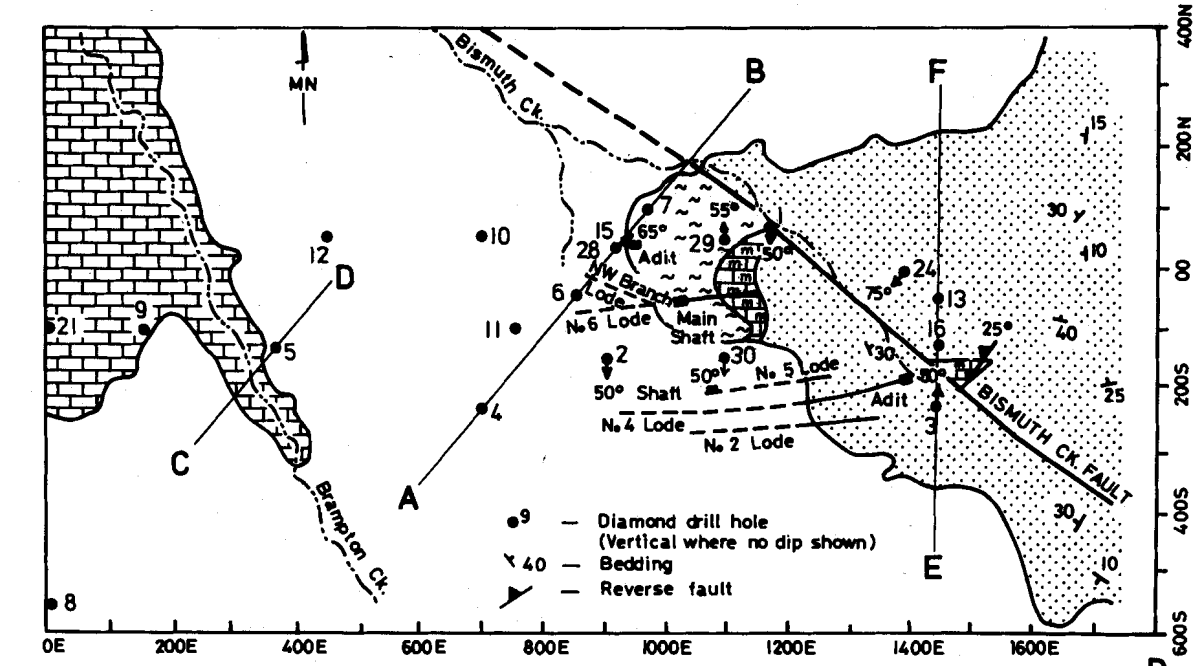
MN
Bismuth Ck.
Brampton Ck.
A
B
C
D
E
F
Adit
NW Branch Lode
No.6 Lode
Main Shaft
50° Shaft
No.5 Lode
No.4 Lode
No.2 Lode
BISMUTH CK. FAULT
9 — Diamond drill hole (Vertical where no dip shown)
40 — Bedding
— Reverse fault
0E
200E
400E
600E
800E
1000E
1200E
1400E
1600E
400N
200N
00
200S
400S
600S

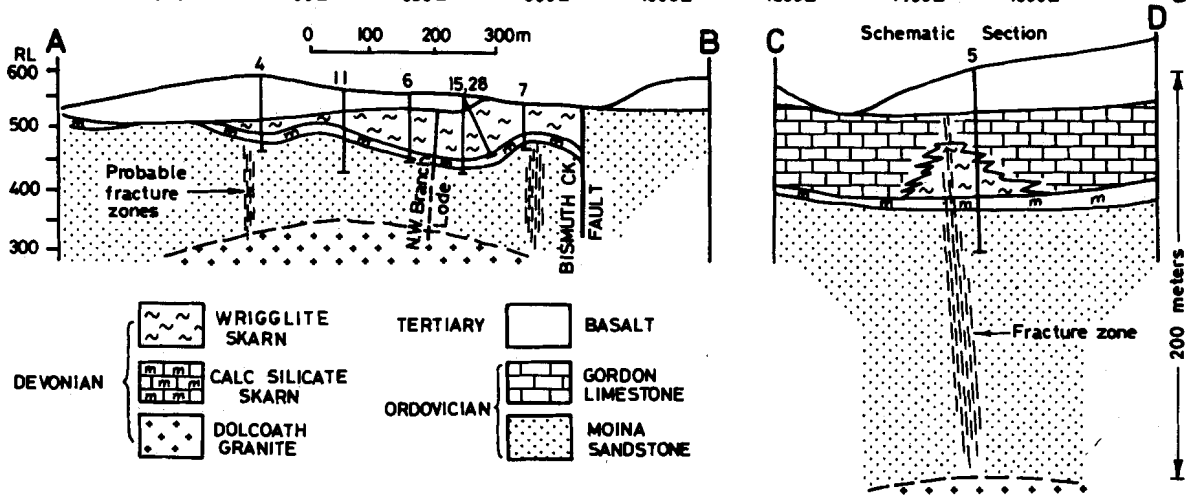
A
B
C
D
RL
600
500
400
300
0 100 200 300m
Probable fracture zones
NW Branch Lode
BISMUTH CK. FAULT
Schematic Section
Fracture zone
200 meters
WRIGGLITE SKARN
CALC SILICATE SKARN
DOLCOATH GRANITE
DEVONIAN
TERTIARY
BASALT
ORDOVICIAN
GORDON LIMESTONE
MOINA SANDSTONE

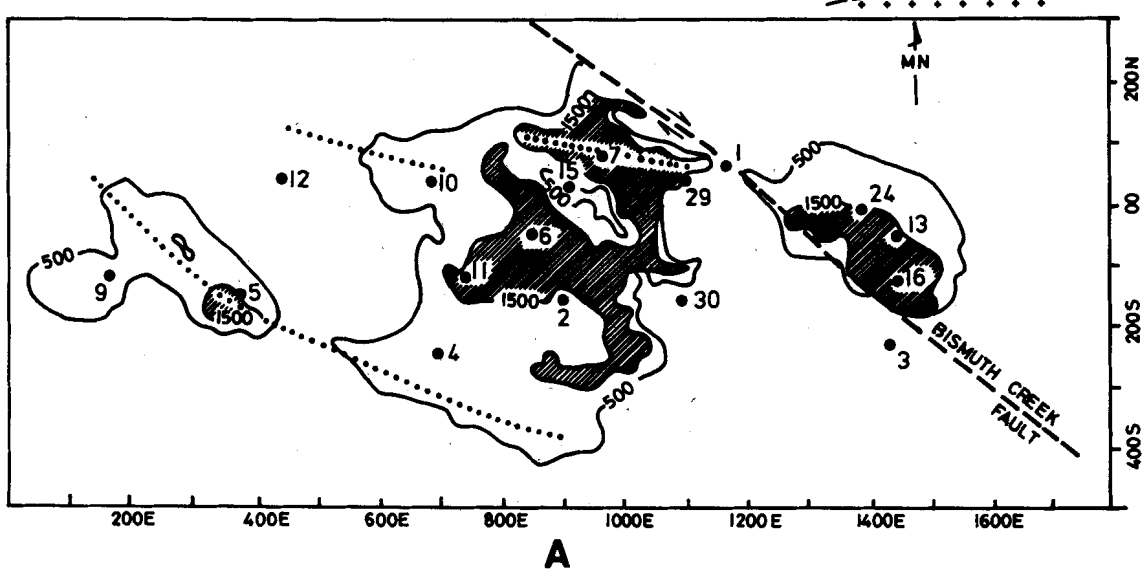
MN
500
1500
BISMUTH CREEK FAULT
200E
400E
600E
800E
1000E
1200E
1400E
1600E
200N
00
200S
400S

A

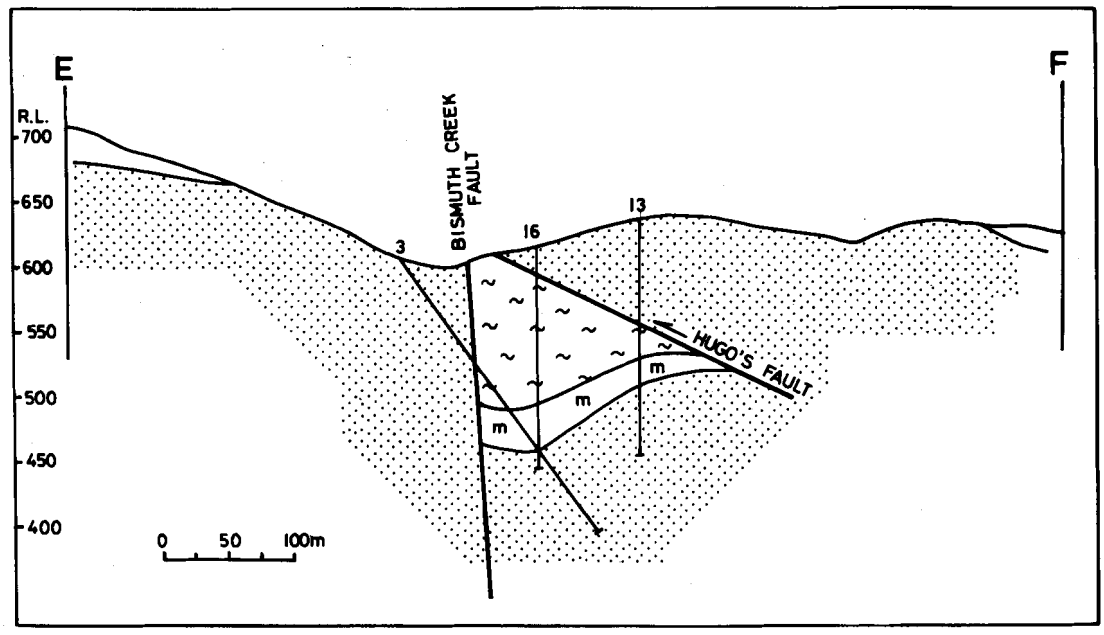

FIG. 1. B. Section E-F is an enlarged section showing skarn occurring beneath a reverse fault.

associated with a major fault. Tertiary basalt covers much of the area.

Granite

Granite has been intersected at a depth of approximately 200 m in diamond drill holes ML-1 and ML-2. Greisenization in the granite in ML-1 decreases downward from its contact at 279 to 317 m (distances down a hole of 50° dip) and consists of a grayish-white-colored zone nearest the contact (zone 1: 279 to 280.8 m), a gray zone (zone 2: 281.8 to 281.8 m), a green zone (zone 3: 281.8 to 292.7 m) and a pinkish-yellow zone (zone 4: 292.7 to 317 m) farthest from the contact. On the basis of color differences, the contacts between zones 1 and 2, and 2 and 3 are abrupt—over 5 cm—whereas that from zone 3 to 4 is less abrupt. Small areas of pinkish (zone 4) greisen appear in zone 3 and greenish (zone 3) greisen in zone 4. This indicates that irregularities of permeability may have existed and may account for minor chemical variations.

In zone 4, the least-altered samples consist of approximately 60 percent quartz, 20 percent white mica, <1 percent brown biotite, 20 percent orthoclase, 8 percent oligoclase, and accessory fluorite, pyrite, rutile, and hematite. By comparison, unaltered Dolcoath granite cropping out in the Forth River Valley 4 km east has an average composition of 35 percent quartz, 5 percent biotite, 40 percent K-feldspar, and 20 percent plagioclase (Gee, 1966), with accessory fluorite and zircon (Jennings, 1963). In zone 4, primary dark brown biotite occurs only as armored relicts in quartz. Fe calculated as Fe^{+2} is 4.451 atoms per molecule (24 oxygens per unit cell), F = 1.126, Ti = 0.431, and Cl = 0.106 with Fe^{+2}/Fe^{+2} + Mg = 91.5 (analysis 8, Table 1).

In zones 3 and 4, two types of white mica coexist having distinctly different compositions. Type 1 is coarse grained with high values of F (0.807 atoms/molecule), Fe(0.846), and Mg(0.123) and with relatively low Si and high Al for muscovite (analysis 4, Table 1). Type 2 in zone 4 occurs as fine-grained masses with low values of F(0.215), Fe(0.415), Mg(0.075), and high Si with lower Al than type 1 (analysis 6, Table 1). The Fe^{+2}/Fe^{+2} + Mg ratio of type 1 is higher than that of type 2 (87.3 vs 84.7). Texturally, type 2 commonly occurs between type 1 mica and unreplaced feldspar relicts. The modal ratio of type 1/type 2 decreases upward until no type 2 occurs in zones 1 and 2. This and the relatively great

FIG. 1. A. Geologic map, cross section, and magnetic anomaly map of the Moina Laminar skarn area. The geologic map shows the location of diamond drill holes. The position of shafts and cassiterite-wolframite-quartz lodes of the Murphy and Shepherd mine are shown. Section A-B is normal to fold trends and to the Bismuth Creek fault and is drawn to scale. Section C-D is schematic showing the probable nature of replacement of the limestone in fracture zones. The magnetic anomaly map is simplified fluxgate data (vertical component of the field) in nanoteslas and shows northwest-southeast and east-west trends.

TABLE 1. Electron Microprobe Analysis of Minerals Present in Greisenized Granite and Quartz Veins

	1	2	3	4	5	6	7	8	9	10	11
SiO_2	44.57	45.25	45.27	44.91	47.92	47.97	50.07	32.60	0.35	1.39	31.68
TiO_2	0.37	0.05	0.04	0.21	0.05	0.03	0.13	3.20	0.50	90.92	0.01
Al_2O_3	28.64	29.99	30.44	29.74	31.96	31.37	28.96	12.87	0.32	1.33	53.18
FeO	6.85	6.63	6.31	6.73	2.73	3.36	1.14	29.73	64.54	4.49	0.03
MnO	0.46	0.22	0.23	0.21	0.09	0.07	0.06	1.65	3.49	0.07	0.03
MgO	0.50	0.22	0.10	0.55	0.28	0.34	1.91	1.56	0.43	0.02	0.02
CaO	0.00	0.00	0.00	0.00	0.27	0.05	0.00	0.00	0.40	0.09	0.00
Na_2O	0.35	0.26	0.22	0.30	0.09	0.16	0.04	0.01	0.13	0.15	0.00
K_2O	10.22	10.19	10.01	10.21	9.24	9.22	10.58	9.11	0.01	0.29	0.02
F	1.90	1.55	1.02	1.70	0.30	0.46	1.38	1.99	0.05	0.09	4.07
Cl	0.02	0.05	0.05	0.02	0.11	0.04	0.01	0.35	0.04	0.07	0.01
Anhydrous total	93.88	94.41	93.69	93.58	93.04	93.07	94.40	93.15	69.76	98.94	96.05
Number of 0 ions	24	24	24	24	24	24	24	24	9	4	24
Si	6.680	6.742	6.793	6.745	7.072	7.087	7.214	5.836	0.040	0.038	3.949
Ti	0.043	0.006	0.005	0.024	0.006	0.004	0.014	0.431	0.000	1.866	0.001
Al^{IV}	1.120	1.258	1.207	1.255	0.928	0.913	0.786	2.164	0.044	0.064	0.051
Al^{VI}	3.941	4.010	4.178	3.833	4.623	4.551	4.133	0.552			7.764
Fe^{+2}	0.859	0.826	0.792	0.846	0.337	0.415	0.137	4.451	5.539[1]	0.102	0.003
Mn	0.059	0.028	0.029	0.027	0.012	0.009	0.007	0.251	0.343	0.002	0.003
Mg	0.112	0.030	0.023	0.123	0.061	0.075	0.410	0.416	0.008	0.001	0.004
Ca	0.000	0.000	0.000	0.000	0.043	0.008	0.000	0.000	0.005	0.003	0.000
Na	0.102	1.937	0.063	0.087	0.027	0.046	0.011	0.000	0.029	0.008	0.000
K	1.954	1.937	1.916	1.956	1.740	1.738	1.947	2.081	0.001	0.005	0.004
F	0.901	0.731	0.484	0.807	0.140	0.215	0.629	1.126	0.018	0.008	4.364
Cl	0.005	0.013	0.013	0.005	0.027	0.010	0.002	0.106	0.007	0.003	0.002

[1] Fe^{+3} not Fe^{+2}

1, type 1: white mica, average of 2, zone 1; 2, type 2: white mica, average of 2, zone 2; 3, type 1: white mica, average of 5, zone 3; 4, type 1: white mica, average of 8, zone 4; 5, type 2: white mica, average of 5, zone 3; 6, type 2: white mica, average of 8, zone 4; 7, white mica, alteration of 11; 8, Fe biotite, average of 3, zone 4; 9, Fe oxide (clot), zone 4 (rock 815, Table 2); 10, rutile, zone 4 (rock 862, Table 2); 11, topaz, in cassiterite-wolframite quartz veinlet. Chemical compositions were determined by means of a Joel JXA-5A electron microprobe with computer control, located at the Department of Geology, University of Melbourne, using a beam current of 0.1 mA and an accelerating potential of 15 kV. The following standards were used: SiO_2, wollastonite and quartz; Al_2O_3, corundum; TiO_2, rutile; Fe total and Ba, anandite; K_2O, potassium tantalite; Mn, Mn metal; Ni, Ni metal; F, fluorite; Cl, halite; and Na, jadeite. The computer program for the reduction of electron microprobe data was written by Mason et al. (1969) with modifications by A. K. Ferguson.

depth suggest that type 2 is not related to any surface alteration process. The occurrence of two coexisting micas may be due to the solid solution of another component such as Li. The Li content of type 1 (sample 799) is 770 ppm, but coexisting types 1 and 2 could not be separated. The Li content of the rocks is, however, relatively low (<700 ppm) (Table 2). The lower F content of type 2 may indicate that this mica formed late in the paragenesis at the expense of unreacted feldspar. Related Mn-rich hematite "clots" (analysis 10, Table 1) and fluorite may represent Fe-biotite relicts.

In zone 3, hematite clots are largely absent and only minor relicts of feldspar remain associated with type 2 mica clots. Also, Fe-biotite armored relicts are absent.

Zone 2 is probably a greisen vein which may originally have been a fault or shear zone prior to and/or during greisenization. It consists largely of coarse-grained type 1 mica (see analysis 2, Table 1), fluorite, quartz, pyrite, minor amounts of rutile (analysis 10, Table 1), and minute cassiterite grains. Throughout the zone there are quartz crystal-filled vugs suggesting high porosity (and permeability?) in the zone.

Zone 1 consists largely of quartz with type 1 mica (analysis 1, Table 1), fluorite, pyrite, and very minor amounts of sphalerite.

Above the granite, quartzite has been greisenized and some greisenized granitic dikes also occur.

The bulk chemistry and densities of 16 samples of the greisenized granite collected at regular intervals are shown in Table 2 with the average composition for each zone. For true comparisons to be made, these rocks should have the same densities. The densities of the samples in Table 2 do vary (e.g., 784 = 2.544 g/cm^3; 780 = 2.826 g/cm^3) and, accordingly, for comparison purposes, molar quantities per 100 cm^3 volume of rock were calculated (Fig. 2). As can be seen, Na_2O and Sr decrease systematically toward the contact representing, in part, the progressive break-

down of plagioclase. K_2O, CaO, Al_2O_3, Fe_2O_3, FeO, TiO_2, H_2O^+, Zn, Cl, Rb, Sn, Ga, Li, Yb, Cu, and to a lesser extent B are all enriched in zone 2. These enrichments reflect the large abundances of muscovite, fluorite, and cassiterite with some base metal sulfides. SiO_2, Zr, Th, U, Y, and Pb decrease in zone 2. MnO increases toward the contact. The inverse trends of Ti and Zr probably indicate that one (Ti?) or both of these elements are mobile in this environment.

Sedimentary rocks

The (meta-) sedimentary rocks of the area consist of the Ordovician Moina Sandstone (intertidal facies?), conformably overlain by Ordovician Gordon Limestone (intertidal to subtidal facies).

The Moina Sandstone is a well-bedded sequence of pale quartz sandstones and quartz siltstones with rare pebbly beds and rare shale. At the top of the sequence more finely grained silty beds predominate over sandy beds. Close to the granite, the sandstone has been recrystallized to a dense compact coarse-grained quartzite. For about 10 m below the skarn the unit consists dominantly of highly fractured dense gray fine-grained quartzite consisting of quartz ± biotite ± chlorite ± magnetite ± clinopyroxene ± amphibole ± fluorite ± calcite. The clinopyroxene is commonly partly altered to amphibole. Unaltered Gordon Limestone is dominantly a fine-grained, compact, pale to dark gray mudstone with well-defined bedding which was slightly disturbed, apparently by burrowing organisms. Particularly toward the base there are thin beds of silty or dolomitic limestone. When unaltered, the bottom transition to the Moina sandstone consists of about 10 m of limestone containing 0.5- to 10-cm-wide interbeds of siltstone, calcareous siltstone, and limestone. The bulk of the limestone is nondolomitic and contains less than 3 percent MgO.

Fracturing and veining

Fracturing and veining of skarn and quartzite is most intense near the contact between quartzite and skarn (Fig. 4A). Alteration of the massive quartzite has occurred out from fractures which are now filled with vein material. Early formed veins were intersected by later ones having different mineralogies and/or abundances of minerals. Thus, for a sample from drill hole SMD 12 at 62 m (see Fig. 1A for location), the general sequence of vein types is amphibole-biotite-muscovite, fluorite-adularia-scheelite, adularia-fluorite-biotite, and calcite-amphibole (Fig. 3B). Only the fluorite-rich fractures, which constitute the largest number, invariably have a magnetite-diopside selvedge separated from the vein by granular diopside (see Fig. 4A). Analyses 8 and 9 (Table 4) are of fractured and veined quartzite. On a 100 cm^3 basis it can be shown that relative to unveined quartzite (see 5 and 6, Table 5 and Fig. 7) the rocks are enriched in Be, Cl, Li, Cu, Zn, Sn, Sr, Rb, Th, W, Ca, Fe^{+2}, Fe^{+3}, K, F, Al, and Mn, with a loss of Si and Y. The fact that the most intense fracturing occurs nearest the lower contact and throughout the skarn but not nearer the granite suggests that the fracturing is produced by a skarn-forming process and is not directly related to the intrusion of the granite. The sequence of vein fillings reflects changing conditions (composition of the fluids, temperature, etc.) during skarn genesis as will be discussed later.

Quartz veins ("lodes" in Fig. 1A) from 0.5 mm to 1 m wide, generally striking east-west and dipping steeply north, are found throughout the quartzite and the lower part of the skarn unit. The widest and greatest abundance of these occur near the skarn-quartzite boundary (see Fig. 1A), although they are reported to have been mined to a maximum depth of 145 m into the underlying quartzite (Jennings, 1965). They were mined for Sn and lesser W until 1956 and consist of quartz containing wolframite, cassiterite, bismuthinite, native bismuth, sphalerite, molybdenite, chalcopyrite, pyrite, scheelite, arsenopyrite, galena, fluorite, topaz, beryl, phlogopite, muscovite, chlorite, and laumontite. Topaz from a cassiterite-wolframite-quartz vein (coordinates 1700E 100S, Fig. 1A) has a high F content (analysis 11, Table 1) and contains high-temperature (430°C, uncorrected for pressure), saline fluid inclusions as will be discussed. In the veins, the Sn:W ratio decreases from 20:12 near the surface (Williams, 1958) to 10:40 at depth (Reid, 1971).

Skarns

Skarn here refers to all calc-silicate-bearing rocks derived from Ca-rich sedimentary rocks. The generalized section consists of a lower calc-silicate skarn overlain by a wrigglite (magnetite-fluorite) skarn. The total skarn unit extends over more than 1 km in its longest dimension and is up to 100 m thick (Fig. 1A). The major magnetic anomalies shown in Figure 1A reflect the major skarn areas, but skarn thicknesses of up to at least 20 m exist below some areas of low magnetic relief (e.g., in drill hole SMD 12). Fortunately the overlying Tertiary basalt is relatively nonmagnetic, but there are pyrrhotite-rich and sphalerite-rich areas of as yet unknown extent which could complicate a simple interpretation of the magnetic picture.

The magnetic picture shows clearly a 300-m lateral displacement of the skarn along the Bismuth Creek fault, though some of this may actually be an apparent lateral movement caused by vertical displacement of shallowly dipping beds. Elsewhere in the

TABLE 2. Compositions of Greisenized Granite and Average of Zones in the Greisen

Sample no.	774	776	779	780	784	788	795	809	812
SiO_2	76.16	73.51	62.64	44.23	74.15	76.96	76.12	76.94	75.52
TiO_2	0.04	0.03	0.05	0.10	0.04	0.04	0.04	0.04	0.04
Al_2O_3	11.21	11.43	18.99	27.86	10.98	12.70	12.86	12.37	12.28
Fe_2O_3	0.00	0.19	1.36	2.15	1.10	0.42	0.70	0.91	0.49
FeO	4.63	4.37	3.78	5.08	4.35	1.12	1.09	0.77	1.54
MnO	0.10	0.17	0.19	0.18	0.26	0.04	0.03	0.03	0.06
MgO	0.10	0.15	0.10	0.35	0.16	0.12	0.14	0.14	0.13
CaO	0.01	1.29	1.68	2.22	0.51	0.41	0.62	0.30	0.46
Na_2O	0.23	0.22	0.30	0.45	0.20	1.38	0.48	0.56	2.03
K_2O	3.68	3.98	6.50	9.61	3.67	4.95	4.52	4.90	5.10
P_2O_5	0.00	0.00	0.00	0.02	0.00	0.05	0.01	0.00	0.00
S	1.17	0.56	0.00	0.54	0.02	0.05	0.21	0.09	0.06
H_2O^+	1.62	1.34	1.56	2.40	0.34	1.76	1.84	1.30	1.08
H_2O^-	0.26	0.15	0.11	0.25	0.35	0.38	0.46	0.93	0.35
CO_2	2.53	3.17	1.58	0.99	3.11	0.37	0.39	0.17	0.93
Total	101.74	100.54	98.84	96.70	99.24	100.76	99.51	99.45	100.07
−S = 0	0.59	0.28	0.00	0.27	0.01	0.03	0.10	0.04	0.03
Total	101.16	100.26	98.94	96.42	99.23	100.73	99.41	99.41	100.04
+F	0.34	1.36	2.27	3.43	0.51	0.46	0.60	0.29	0.41
Total	101.50	101.61	101.11	99.85	99.74	101.19	100.01	99.70	100.45
Sr	3.4	5.1	5.5	8.4	4.1	6.2	6.7	7.5	8.7
Y	78.4	97.3	0	0	95.9	785.7	212.0	156.7	84.0
Pb	200.0	25.2	12.2	14.9	214.4	114.5	45.6	57.9	38.8
Th	48.5	52.1	14.9	3.0	45.1	66.5	61.0	58.5	57.9
U	18.8	7.7	3.4	2.1	23.3	18.9	39.2	32.7	32.4
Rb	866.0	1,003.2	2,480.2	2,816.0	563.1	709.2	698.9	672.8	661.4
Zr	107.4	104.0	34.6	21.0	111.4	112.5	124.5	121.1	118.0
Nb	34.4	22.7	35.0	86.8	36.0	49.9	53.1	53.1	38.3
Ga	25	27	69	126	23	25	25	23	24
Be	25	30	40	60	50	30	40	30	50
Sc	0	0	0	30	3	0	0	3	3
Mo	0	0	3	3	15	0	0	0	10
Yb	10	25	25	40	10	80	25	30	20
Sn	85	360	330	560	36	50	55	46	50
Li	250	250	300	700	200	150	150	100	150
Gl	48	51	77	82	34	<20	39	38	<20
Ni	48	52	92	136	42	128	56	47	38
Cu	82	111	2	51	72	51	42	24	31
Zn	56	37	36	35	502	51	21	8	5
W	ND	20	ND	ND	ND	ND	ND	ND	ND
B	0	0	0	0	0	0	0	0	0
Density	2.6612	2.7268	2.7238	2.8265	2.5443	2.6180	2.6409	2.5989	2.6369

The major oxides SiO_2, TiO_2, Al_2O_3, Fe_{total}, MnO, MgO, CaO, P_2O_5, and SO_3 were analyzed by X-ray spectroscopy; K_2O and Na_2O by flame photometry; H_2O and CO_2 by weight differences on absorption of phosphorus pentoxide and "carbosorb," respectively; FeO by colorimetry at La Trobe University. F was determined by specific ion electrode analyses at Comalco Laboratories (Thomastown, Victoria, Australia). B and Li were determined by wet chemical means at the Australian Mineral Development Laboratories (Amdel). Be, Sc, B, and Mo were done spectographically; Sn and W were done by X-ray fluorescence at Amdel. Sr, Y, Pb, Th, U, Rb, Zr, Nb, Ga, Cl, Ni, Cu, and Zn were done by X-ray fluorescence at La Trobe University.

Assigning limits to the possible analytical errors for these analyses is problematical. For the trace elements the following detection

Moina area there is evidence of the opposite sense of displacement on the fault, and so it is possible that there has been more than one episode of movement. The magnetic picture also shows northwest trends and east-west trends. The northwest trends seem to correlate with known folding and/or faulting with northwest axes in an area close to the Bismuth Creek fault and the east-west trends seem to correlate with zones of tension fractures, which would have acted as the main part of the hydrothermal plumbing system. The major quartz lodes are part of this east-west system (Fig. 1A). The skarn east of Bismuth Creek is compositionally variable and lies beneath a reverse fault (Fig. 1B).

Three general types of calc-silicate skarn occur, namely, (a) a distinctive pale green pyroxene skarn,

from Diamond Drill Hole ML-1 (The sample positions are those shown in Figure 2.)

815	825	830	839	856	862	870	Avg. zone 1	Avg. zone 2	Avg. zone 3	Avg. zone 4
77.69	76.72	78.02	75.22	75.54	76.11	76.64	74.84	53.44	76.04	76.43
0.04	0.03	0.04	0.03	0.04	0.03	0.03	0.03	0.07	0.04	0.04
10.52	11.54	11.19	12.09	12.17	11.94	11.84	11.32	23.43	12.33	11.70
0.92	0.45	0.48	0.41	0.29	0.09	0.00	0.10	1.76	0.78	0.26
1.45	1.84	1.05	1.57	1.36	1.35	1.32	4.50	4.43	1.83	1.44
0.08	0.04	0.03	0.07	0.05	0.03	0.03	0.14	0.19	0.09	0.05
0.08	0.04	0.06	0.15	0.13	0.04	0.07	0.13	0.23	0.14	0.09
0.52	0.60	0.54	0.55	0.53	0.48	0.51	0.65	1.95	0.46	0.52
1.83	1.86	2.47	2.40	2.76	2.54	2.93	0.23	0.38	0.66	2.35
4.19	4.83	4.24	4.81	4.87	5.09	4.99	3.83	8.06	4.51	4.77
0.00	0.00	0.00	0.00	0.00	0.00	0.00	0.00	0.01	0.02	0.00
0.07	0.02	0.03	0.04	0.00	0.04	0.00	0.87	0.27	0.09	0.03
0.78	0.99	1.08	0.66	0.71	0.50	0.99	1.48	1.98	1.31	0.85
0.18	0.29	0.19	0.27	0.21	0.27	0.31	0.21	0.18	0.53	0.26
1.07	0.83	0.72	0.74	0.61	0.56	0.66	2.85	1.29	1.01	0.77
99.42	100.09	100.13	99.02	99.27	99.08	100.34	101.14	97.77	99.74	99.68
0.03	0.01	0.01	0.02	0.00	0.02	0.00	0.44	0.14	0.15	0.02
99.39	100.03	100.12	99.00	99.27	99.06	100.34	100.70	97.63	99.69	99.66
0.38	0.47	0.38	0.37	0.38	0.33	0.70	0.35	2.85	0.37	0.43
99.77	100.55	100.40	99.37	99.65	99.39	101.04	101.05	100.48	100.16	100.09
8.7	8.5	9.1	9.0	10.0	9.7	9.5	4.3	7.0	6.1	9.2
86.9	77.6	126.6	163.9	118.1	142.2	111.9	87.9	0	312.6	113.9
53.2	20.7	23.2	26.1	36.8	32.1	31.4	112.8	13.6	108.1	32.8
59.0	39.5	50.0	48.0	52.2	52.5	44.9	50.3	13.6	57.8	50.6
51.2	14.7	13.3	16.9	11.6	52.9	15.6	13.3	2.8	28.5	26.1
532.8	542.3	557.0	617.0	628.1	636.0	613.1	934.6	2,648.1	661.0	598.5
109.3	92.1	105.4	119.8	105.9	123.8	97,3	105.7	27.8	117.4	109.0
55.5	61.8	53.1	51.9	43.5	58.8	31.6	28.6	60.1	48.0	49.3
19	25	21	20	23	21	22	27	97.5	24.0	21.9
30	50	30	30	30	50	40	28	50	37.5	38.8
3	0	0	0	0	0	0	0	15	2	1
59	0	30	0	0	7	0	0	3	4	12
20	20	25	25	15	30	15	18	33	36	21.3
40	4	44	50	40	26	30	222.5	445.0	47	40.5
150	100	100	100	100	70	80	250	500	137.5	106.3
<20	20	20	20	20	39	21	50	79.5	27.8	7.5
30	27	38	43	40	40	33	50	114.0	68.3	36.1
181	3	8	9	16	15	15	96.5	27	47.3	34.8
7	11	5	4	6	4	3	46.5	36	146	6
				50		30	20	110		40[1]
0	0	0	0	0	0	0	0	0	0	0
2.6536	2.6155	2.6448	2.6183	2.6259	2.6074	2.6034	2.6940	2.7752	2.6005	2.6257

levels in ppm are suggested (R. Price, pers. commun.): Cu (0.5), Zn (0.5), Rb (0.4), Sr (0.3), Y (0.3), Zr (0.8), Nb (0.9), Pb (1.2), V (1.0), Cr (0.9), Ba (3.7), La (1.3), and Ce (4.0). The values for Mo, W, Th, and U are unknown but most likely are of the same order as the other elements (1.0 ppm or so). Analytical errors of major elements as suggested by Norrish and Hutton (1969) for X-ray spectroscopy-derived values are as follows (coefficient of variation of mean values percent) SiO_2 (0.30), TiO_2 (1.1), Al_2O_3 (0.63), Fe_2O_3 (0.71), MnO (2.4), MgO (0.92), CaO (0.81), and P_2O_5 (1.6). Values for Na_2O, K_2O, and SO_3 are (again) probably of the same order. Detection levels for the other trace elements in ppm are B (3), Yb (1), Mo (3), Sc (3), Y (10), Be (1), Sn (20), W (20), and Li (5). The samples were crushed in an Mo-W-free Mn-Cr Sieb mill, thus introducing the possibilities of Mn and Cr contamination.

(b) a garnet-vesuvianite-fluorite ± wollastonite ± amphibole ± epidote ± magnetite skarn, and (c) a wollastonite skarn (see Fig. 4B for types a (GS) and b (PS)). Type a consists of thin beds up to 3 cm wide having irregularities along strike but generally having a sharp contact with type b. Thin pyroxene skarn units are common nearest the lower contact of the overall skarn unit, becoming less common higher in the column. These represent replacement of calcareous siltstone interbeds which occur unaltered about 100 m west of SMD 21 (Fig. 1A) in the adjacent unreplaced Gordon Limestone and are bioturbated, with irregular bedding. This feature is retained in the skarn (Fig. 4C) which suggests that, apart from fracturing, the replacement of the units was a relatively passive event. In all of the skarn units, bimetasomatic zon-

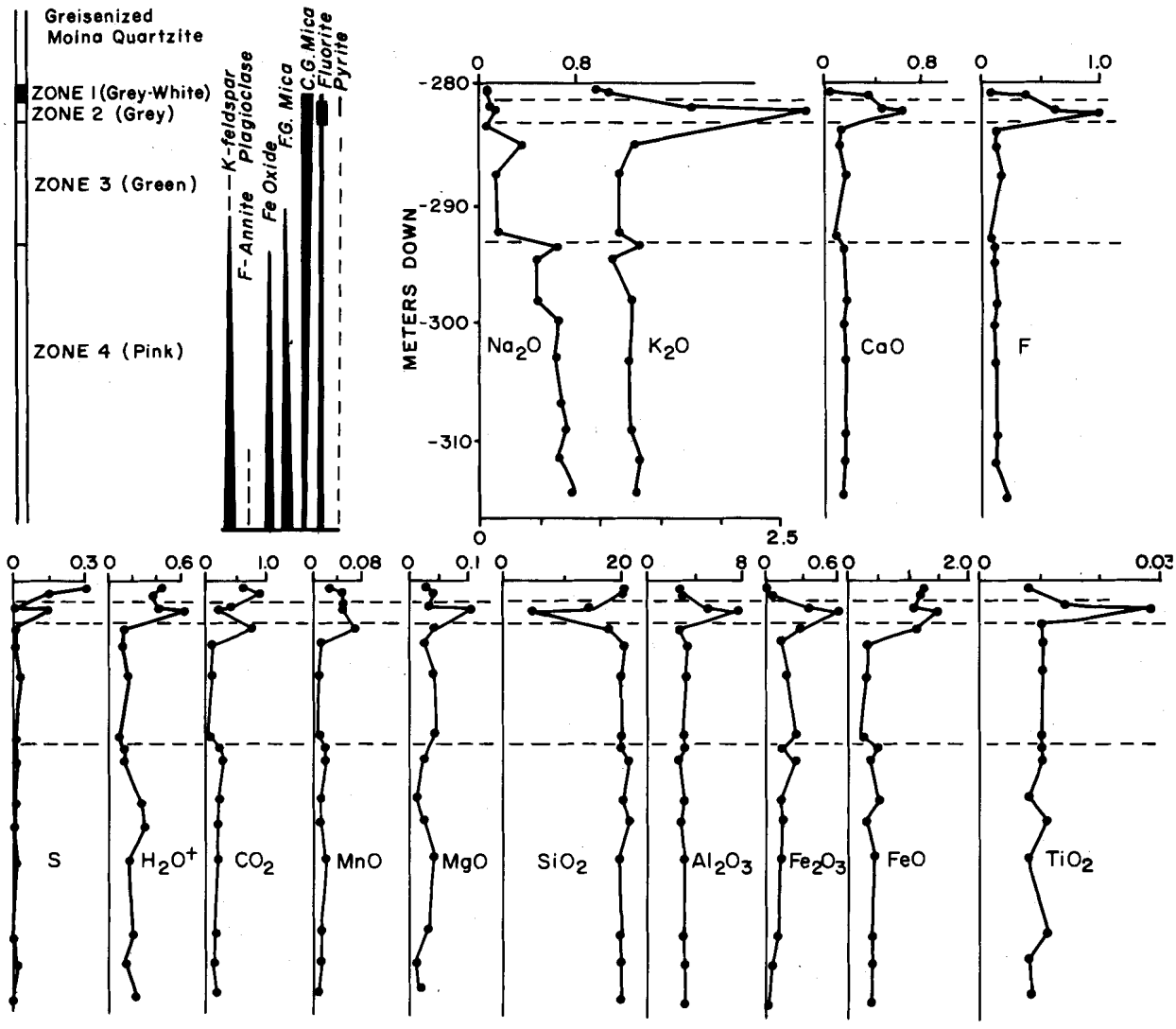

FIG. 2. Chemical variations of major and minor elements from the granite (greisen)-quartzite contact from 280 m down to 316 m in drill hole ML-1 (see Fig. 1 for location). The zones and mineralogy are explained in the text. The values are in moles per 100 cm^3 of rock (thus corrected for density differences). The values were calculated from those in Table 2.

ation is generally absent, reflecting the lack of major chemical or permeability gradients.

The pyroxene skarn consists mainly of fine-grained (<0.2 mm) diopside-hedenbergite pyroxene (ratio 40:60) with very minor amounts of fluorite and garnet. By comparing pyroxene skarn from SMD 5 at 56 m with similar interbeds beyond SMD 21 in unreplaced Gordon Limestone, (Table 4), it can be seen that Na, Sn, F, W, Zn, and Fe were added to the former (7, Table 5). This change could not have been produced solely by thermal metamorphism and indicates F metasomatism.

The second skarn, type b, occurs mainly near the base and in minor amounts interbedded with recrystallized limestone directly above the wrigglite skarn. All gradations exist but garnet is invariably present in large proportions. The garnet is andradite-grossularite (analyses 8 and 9, Table 3) and has concentric color zoning accentuated by anomalous anistropy in polarized light. Values of Sn of up to 0.70 weight percent were found in garnet. The pyroxene interstitial to and occurring as inclusions in garnet is diopside-hedenbergite (analysis 4, Table 3), whereas the accompanying vesuvianite is relatively Fe and F rich (analysis 1, Table 3). Fe-rich hornblendic amphibole (analysis 12, Table 3) and epidote occur replacing

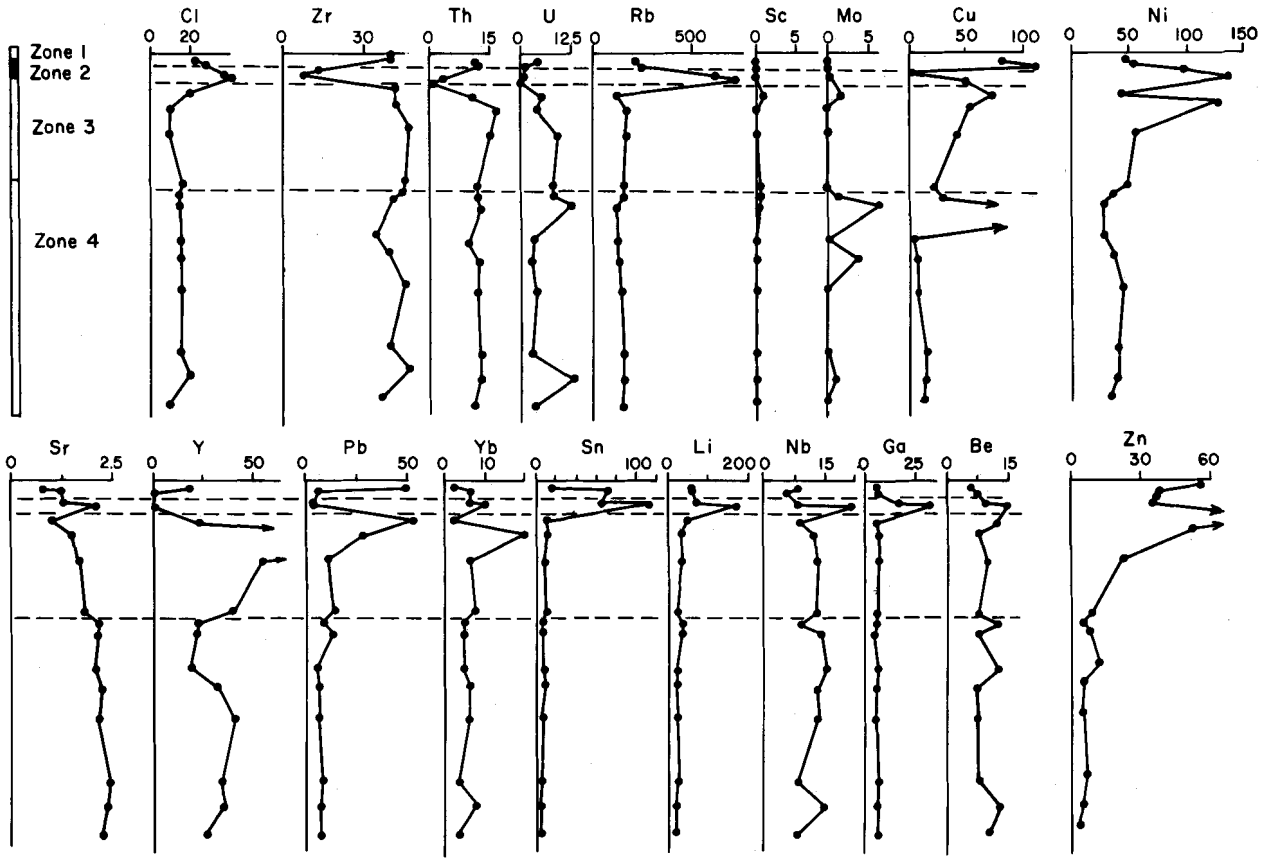

FIG. 2 (cont.)

pyroxene, vesuvianite, and garnet. Interstitial fluorite and adularia occur, occasionally with epidote and calcite in pods up to 2 cm long. Magnetite, scheelite, and pyrite occur as minute grains (to 0.1 mm across), but no cassiterite was observed.

Evidence that this skarn has formed from Gordon Limestone (marble) occurs in some cases (Fig. 4E). Bulk chemical analyses of garnet skarn (6, 11, and 18, Table 4) recalculated on a molar basis per 100 cm^3 volume (8, Table 5, and Fig. 7) show that relative to limestone (17 and 19, Table 4), Sn, H, U, Y, Zn, Li, Cl, Be, Si, Fe^{+2}, Fe^{+3}, F, Al, Mn, and B were added whereas Sr, C, and Ca were removed. The light elements Li, Be, B, and Cl are particularly enriched in garnet skarn overlying the wrigglite skarn (see Fig. 4E). Specific boron minerals were not found.

As in the quartzite, veinlet-filled fractures in calc-silicate skarn show a sequential deposition so that for SMD 5, 56 m down, the sequence is veins rich in: (1) muscovite, (2) potassium feldspar (adularia)-fluorite, and (3) calcite (in Fig. 4B and C). The sequence may be only partly shown in any one sample so that in Figure 3A only (2) above is present. The margins of fluorite-bearing veins commonly show marginal alteration to magnetite ± amphibole of garnet and pyroxene skarn (i.e., Fig. 4B).

Calc-silicate skarn type c consists mainly of wollastonite (>80 vol %) with lesser amounts of garnet, pyroxene, vesuvianite, and fluorite. It is probably a variation of type b in representing the metamorphism of extremely quartz-rich impure limestone interbeds, which occur up to 3 m thick. Like the other calc-silicate skarns, it is enriched in F, Sn, Fe, W, and Cl (10 and 14, Table 4).

The main skarn type is a dark, heavy, fine-grained rock showing chaotic laminar patterns of alternating light and dark lamellae which are up to 0.5 mm wide. The rock type has been called "ribbon rock" skarn (Jahns, 1944a), "rhythmically banded rock" (Shabynin, 1977), "wrigglite" skarn (Askins, 1975), and "apocarbonate greisen" (Govorov, 1958).

The skarn here called wrigglite skarn occurs first as thin interbeds within the upper part of the lower calc-silicate skarn unit (see Fig. 5A). Higher in the column wrigglite skarn occurs interbedded with pyroxene skarn (Figs. 5B and 4C) but generally not with

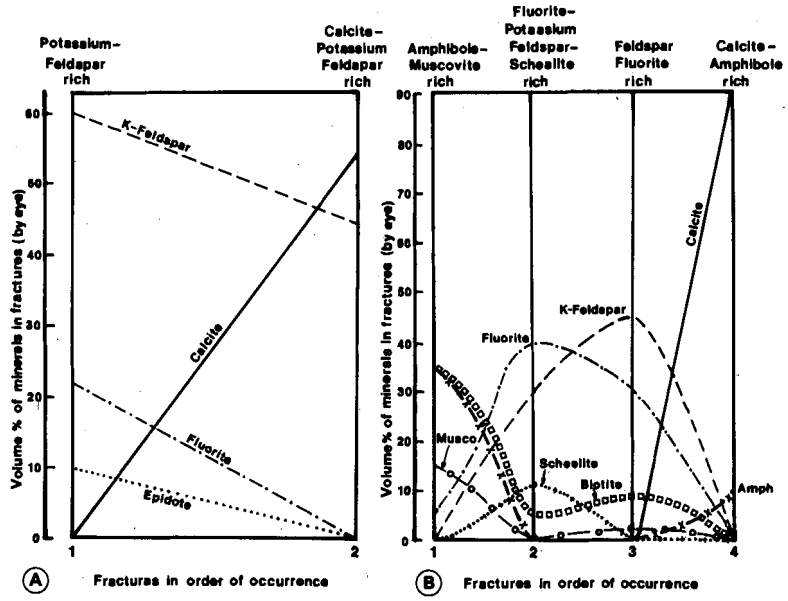

FIG. 3. Graphs showing the mineral contents of sequentially deposited veins in quartzite (B, SMD 5, -65 m), calc-silicate skarn (C, SMD 12, -65 m) and laminar skarn (A and D, SMD 5, -46.2 m). The vein contents were estimated by eye. In most cases between three to ten veins of the same period were averaged to produce the graphs.

garnet skarn. The wrigglite skarn terminates upward against unreplaced marble (where it is not removed by erosion) and septa of skarn occur along fractures extending into the marble (Figs. 5C and D).

The lamination is closely related, and parallel, to fractures (Figs. 5C and D), not bedding (Fig. 5B). In some cases the skarn-marble contact is irregular enough to produce embayments (Fig. 5D) or even pockets of unaltered material. These latter are interpreted eventually to form augen-type structures ("1" in Fig. 5C and "3" in Fig. 5B) or foldlike areas as in Figure 6A. The augen often occur where two or more fractures intersect (Figs. 5C, 4C, and 4D).

The normal primary mineralogy of the wrigglite skarn is magnetite in the dark lamellae and vesuvianite + fluorite in the light-colored lamellae. More rarely, adularia + fluorite and pyroxene ± garnet + fluorite and pyroxene ± garnet + fluorite from the light-colored lamellae. Minor cassiterite occurs, particularly in the magnetite layers, and minor Sn-rich sphene, scheelite, and bismuthinite crystals occur scattered throughout. Molybdenite, sphalerite, pyrite, scheelite, cassiterite, amphibole, bismuthinite, adularia, topaz, unusual K-Ca silicates (on which study is still in progress), and laumontite occur in veinlets. As seen in Figure 6A, the dark layers need not be continuous but pinch and swell making the exact classification of which minerals belong to which lamellae difficult.

Vesuvianite has Fe > Mg (analysis 3, Table 3) and high F (2.369 atoms per formula of 78 oxygens). Pyroxene is rarely found in the light layers, but when it is present it is hedenbergitic (i.e., Fe/Fe + Mg = 0.619, analysis 5, Table 3). This is in sharp contrast to diopsidic pyroxene in accompanying garnet skarn (analysis 4, Table 3). Adularia + fluorite wrigglite probably occur only where high Sn values are found (>0.4 % Sn?). The adularia has few impurities (analysis 16, Table 3). Tin values of 6.31 weight percent are found in rare Sn-rich sphene. Magnetite contains little Sn or W (analysis 15, Table 3) whereas cassiterite, which forms irregular patches up to 15 μm in diameter, contains less than 2.00 weight percent FeO.

As in the quartzite and lower calc-silicate unit, the wrigglite skarn has numerous intersecting fractures and veinlets. For example, in a sample from SMD 5 at 46.5 m (Fig. 3D) the general sequence is veins rich in (1) garnet + fluorite, (2) adularia + fluorite (+ to 2% topaz and 8% scheelite), and (3) fluorite + adularia.

The alteration of the primary wrigglite skarn to form amphibole and/or sulfide-rich equivalents occurs at Moina, as in many skarns throughout the world. The distribution of alteration in the skarn is difficult to define because of the limited number of drill holes and poor surface exposure. Variable amounts of amphibole (±sulfide) alteration occur throughout. In some cases the wrigglite skarn may

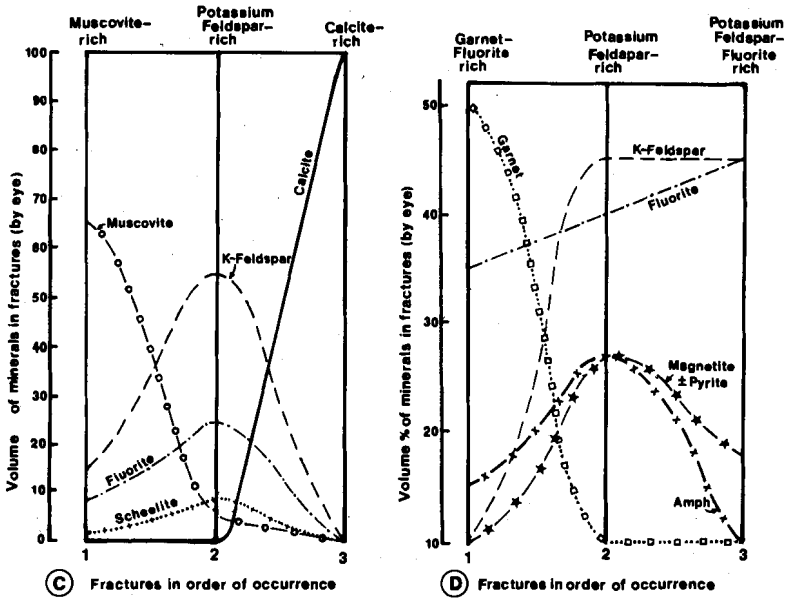

FIG. 3. (cont.).

be altered producing an amphibole-rich area having sharp contact with unaltered skarn (e.g., at "2", Fig. 5D); in others magnetite ± cassiterite relict layers are retained in an amphibole-Fe sulfide matrix. Apart from intermittent alteration throughout the skarn, major areas are known to occur in SMD 9 at the skarn extremity where there is a pyrrhotite-rich skarn and in SMD 13 near the Bismuth Creek fault, beneath a reverse fault, where there is a coarse-grained, sphalerite-rich rock. In both examples, but particularly in the former, relict wrigglite structure occurs with a superposition of a later structure consisting of plates of hematite (SiO_2 = 0.021 moles, CaO = 0.009 moles per 3 oxygens) with marginal Fe-F biotite (analysis 13, Table 3 and Fig. 6D). Amphibole is Fe rich with considerable K + Na (analysis 10, Table 3). Pyrrhotite has the composition $Fe_{0.955}S$ in sample SMD 9 at 97.2 m (Figs. 5F and 6D) whereas hematite (0.027 moles SiO_2 per 3 oxygens) occurs with chalcopyrite.

Near the Bismuth Creek fault the replacement of wrigglite skarn by base metal sulfides, Fe sulfides, and hematite is common (Fig. 5E). Sphalerite in sample SMD 16 at 65 m, has the composition $Zn_{0.863}Fe_{0.164}Mn_{0.020}S_{1.067}$ whereas coexisting pyrrhotite has the composition $Fe_{0.936}S$ and hematite has 0.008 moles SiO_2 (3 oxygens per formula) as impurities. Garnet (and vesuvianite?) alter to hematite + quartz (Fig. 6B); pyroxene, to amphibole (Fig. 6C) and magnetite to sulfides. The amphibole in the alteration is similar to that found in less-altered wrigglite skarn (analyses 11 and 12, Table 3).

Mass Balance Relationships

Mass balance calculations were done to gain some insight into the amount of materials added by the mineralizing solution on traversing the rock units and to see if the constituents were produced by either redistribution in the skarn column, derivation from the quartzite column, or derivation from the greisenized granite. Most of the trace element contents of the skarn are so anomalously high that these could not have been produced by redistribution within the columns and rock types analyzed. To account for density differences, the mass balance calculations for major constituents are shown in Table 5 on the basis of molar changes per 100 cm^3 of rock. Columns 1 to 3 and 5 to 11 are for changes of rock compositions caused by replacement from a previous rock type whereas columns 4 and 12 represent the gains and losses to the fluid from the greisenized granite (column 4) and the skarn (column 12). As can be seen in Figures 2 and 7, when the fluid traversed and reacted with the column of granite, the solution gained Si, Na, and K whereas all other major constituents were lost. For the skarn column, including some quartzite, the solution gained only Ca, a minute amount of P, and large amounts of CO_2. The major constituents added to the greisenized granite column are Al, Fe^{+2}, Fe^{+3}, S, and F; Si, Al Fe^{+2}, Fe^{+3}, Mg, Na, K, S, H_2O, and F were added to the skarn column. Much Si could have been added when the solutions traversed the quartzite (column 5), but clearly most

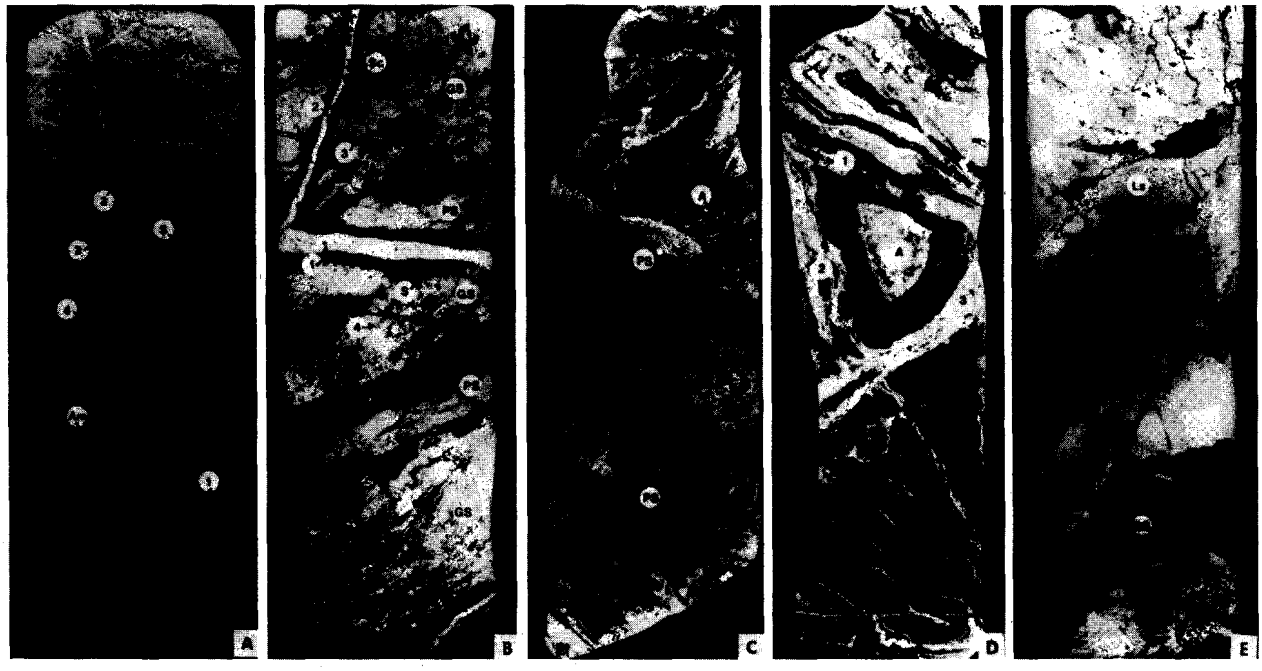

FIG. 4. Examples of drill core from an idealized section through the skarn layer at Moina. The core is approximately 4 cm wide.

A. Photograph of intensely fractured and veined quartzite immediately beneath the skarn units (SMD 5, -62 m). Numbers 1 to 4 = the sequence of vein fills described in the text; S = the magnetite-diopside selvage found at fluorite-rich vein margins described in the text; Am = to amphibole (-epidote)-rich pods.

B. Transmitted light photo of basal skarn showing alternating garnet (GS) and pyroxene skarn (PS) units (SMD 5, -56 m). Numbers 1 to 4 = the sequential nature of intersecting veins; Sc = scheelite grains observable in vein 2; S = the magnetite (-diopside) selvage peripheral to the fluorite-bearing veins (1 and 2).

C. Transmitted light photo of alternating layers of wrigglite skarn and pyroxene skarn (PS) common near the base of the main wrigglite skarn unit. A = a concentrically zoned area of wrigglite skarn. An enlargement of this wrigglite skarn-pyroxene skarn contact is shown in Figure 5B (SMD 12, -101.28 m).

D. Transmitted light photo of wrigglite skarn showing sequential vein fillings (1 to 3) and granular skarn area A (SMD 5, -46.5 m). The latter consists of garnet + fluorite + pyrite.

E. Transmitted light photo of garnet (+ vesuvianite + fluorite) skarn-marble. The skarn is enriched in B, Li, etc., but is not wrigglite. It is a replacement of undisturbed limestone with dolomitic siltstone interbeds.

of the constituents that must have been added to produce the relatively thin skarn column of SMD 12 could not have been derived solely by alteration of quartzite or greisenization of an amount of granite equivalent to the column studied in drill hole ML-1. Also, the skarn overlying adjacent areas of ML-1 is much thicker than that found in SMD 12.

Distribution of Economic Constituents

In the course of exploration by Comalco Limited, approximately 5,000 analyses of Pb, W, Bi, Sn, Mo, Cu, Zn, Be, Sc, Y, Cd, In, Ge, Au, and Ag were done of drill cores SMD 4, 11, 6, 15, and 7 (traverse 1, section line A-B in Fig. 1A) and ML-3, -16, and -13 (traverse 2, section line E-F in Fig. 1A) by the Australian Mineral and Development Laboratories (AMDEL). These are traverses both out from and across the Bismuth Creek fault. The data were analyzed by computer to see (a) the degree of correlation between all possible element pairs, (b) whether there is a relation between the concentration of an element and depth, and (c) whether there is a lateral relation of concentration and proximity to the Bismuth Creek fault. Correlation coefficients were calculated relative to a linear model. Scatter can result from the data not filling a linear model, analytical variation, and the fact that the analyses were done on different skarn rocks and quartzite where density differences were not accounted for. The correlation coefficient data of (a) above shows (Table 6) that elements fall approximately into two groups, namely, (1) Be, F, Sn, and Ag and (2) Zn, Cd, In, Ge, Au, and possibly Bi. The

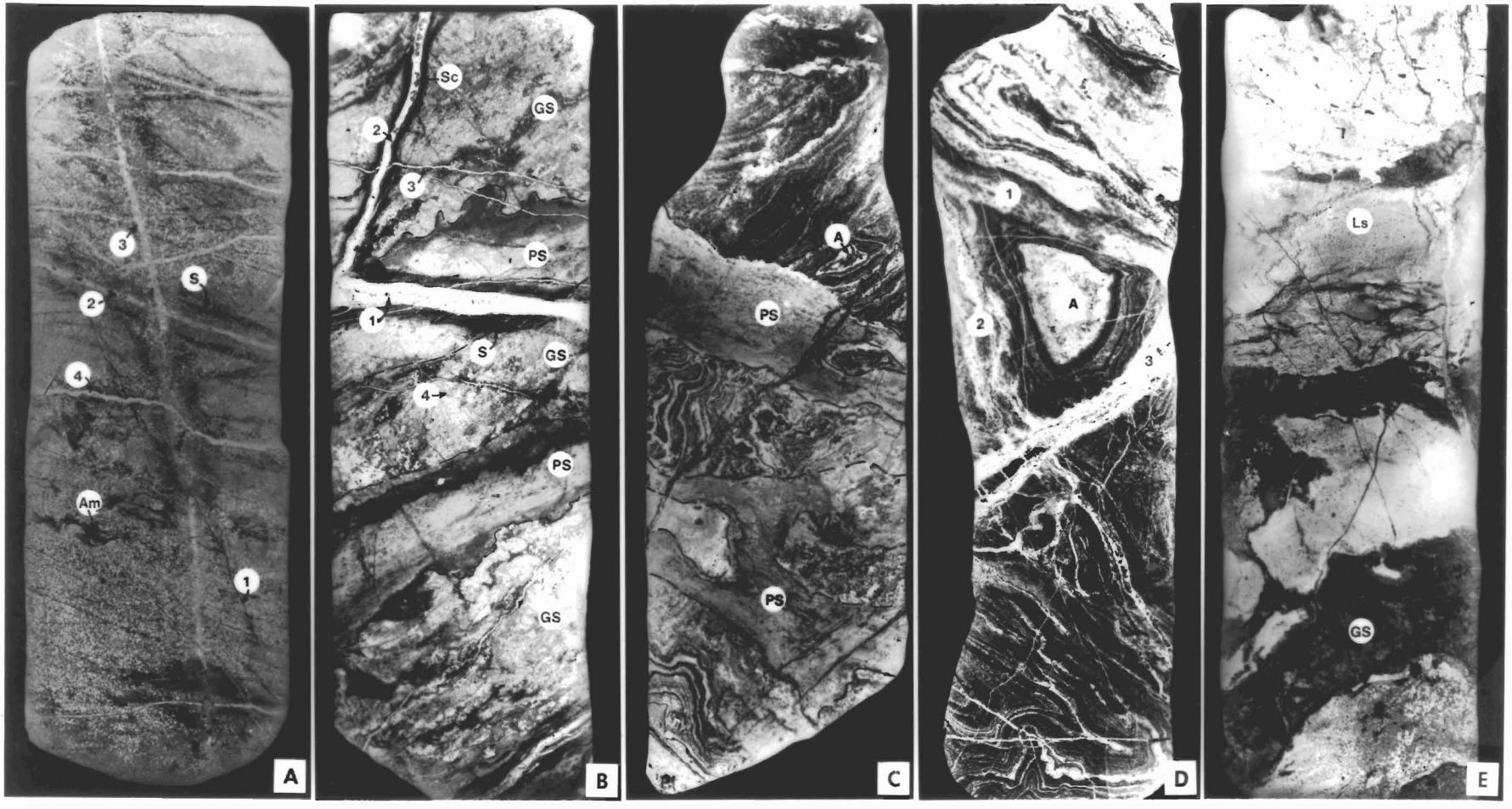
3
S
2
4
Am
1
A
Sc
GS
2
3
PS
1
S
GS
4
PS
GS
B
A
PS
PS
C
1
A
2
3
D
Ls
GS
E

TABLE 3. Composition of Representative Skarn Minerals

	1	2	3	4	5	6	7	8	9	10	11	12	13	14	15	16
SiO_2	36.87	35.19	34.21	53.07	48.94	37.62	37.21	36.89	37.01	36.80	36.55	39.14	34.90	45.61	0.81	66.42
TiO_2	0.07	0.08	0.20	0.00	0.07	0.17	0.20	0.22	0.56	0.20	0.25	0.34	0.00	0.00	0.06	0.02
Al_2O_3	13.70	15.64	13.65	0.19	0.37	5.97	6.09	6.97	8.29	11.54	13.23	14.44	10.90	30.59	0.20	18.73
FeO	5.43	3.98	6.62	4.97	18.33	22.02[1]	21.12[1]	22.29[1]	20.64[1]	27.14	26.16	23.83	36.19	6.76	51.14[1] 46.02	0.32
MnO	0.75	0.83	1.20	0.27	2.83	1.79	1.00	1.86	2.41	0.83	1.42	1.26	1.77	0.00	0.34	0.00
MgO	3.00	2.28	2.15	15.01	4.74	0.09	0.08	0.00	0.01	3.39	2.62	2.00	3.40	0.53	0.00	0.07
CaO	35.19	35.11	35.84	24.86	22.68	31.78	32.51	31.35	31.25	11.22	9.64	11.05	0.15	0.00	0.25	0.00
Na_2O	0.01	0.04	0.02	0.04	0.15	0.05	0.09	0.00	0.01	1.53	1.49	0.28	0.00	0.28	0.01	0.01
K_2O	0.00	0.01	0.04	0.01	0.00	0.02	0.02	0.00	0.02	2.22	2.93	2.25	8.10	10.77	0.00	13.01
F	1.70	1.35	1.40	0.11	0.22	0.23	0.31	0.31	0.32	0.60	0.45	0.29	2.22	2.89	0.00	0.00
Cl	0.24	0.23	0.17	0.02	0.00	0.02	0.06	0.00	0.05	0.52	0.61	0.62	0.24	0.00	0.00	0.00
Anhydrous total	97.05	94.84	95.62	98.56	98.34	99.76	98.69	99.89	100.57	95.99	93.35	95.50	97.78	97.43	98.83	98.58
Number of 0 ions	78	78	78	6	6	12	12	12	12	24	24	24	24	24	4	
Si	19.014	18.558	18.304	1.986	1.976	5.978	6.104	5.992	5.943	6.288	6.268	6.608	6.044	6.439	0.033	12.168
Ti	0.056	0.063	0.081	0.000	0.002	0.020	0.025	0.027	0.068	0.026	0.032	0.026	0.000	0.000	0.002	0.003
Al^{IV}	8.330	9.724	8.611	0.002	0.018	0.022	0.00	0.008	0.057	1.712	1.732	1.392	1.956	1.561	0.010	4.045
Al^{VI}				0.000	0.000	1.096	1.178	1.327	1.512	0.614	0.943	1.583	0.269	3.530		0.000
Fe^{+2}	2.342	1.755	2.962	0.156	0.619	0.000	0.000	0.000	0.000	3.878	3.752	3.878	5.228	0.000	1.557	0.050
Fe^{+3}	0.000	0.000	0.000	0.000	0.000	3.015	2.607	2.725	2.491	0.000	0.000	0.000	0.000	0.718	1.557	0.000
Mn	0.328	0.371	0.544	0.009	0.097	0.241	0.139	0.256	0.312	0.120	0.206	0.120	0.260	0.000	0.012	0.000
Mg	2.306	1.792	1.714	0.837	0.285	0.021	0.020	0.000	0.002	0.863	0.670	0.863	0.877	0.111	0.000	0.019
Ca	19.446	19.840	20.548	9.997	0.981	5.411	5.714	5.457	5.377	2.054	1.771	2.054	0.028	0.000	0.011	0.000
Na	0.010	0.041	0.021	0.003	0.006	0.015	0.014	0.000	0.003	0.507	0.495	0.507	0.000	0.076	0.000	0.002
K	0.000	0.006	0.013	0.000	0.000	0.004	0.002	0.000	0.002	0.484	0.641	0.484	1.788	1.939	0.000	3.041
F	2.772	2.251	2.369	0.011	0.028	0.031	0.161	0.159	0.163	0.324	0.244	0.324	1.215	1.290	0.000	0.000
Cl	0.210	0.205	0.154	0.002	0.000	0.005	0.017	0.000	0.014	0.150	0.177	0.150	0.070	0.000	0.000	0.000

[1] = Fe_2O_3 instead of FeO

Analyses were done as explained in caption of Table 1. 1, vesuvianite: SMD 5, −56 m, in calc-silicate skarn; 2, vesuvianite: SMD 12, −104.18 to −104.29 m, lower calc-silicate skarn; 3, vesuvianite: SMD 12, −93.00 to −93.09 m, wrigglite skarn; 4, pyroxene: SMD 5, −56 m, in calc-silicate skarn; 5, pyroxene: SMD 12, −93.00 to −93.09 m, wrigglite skarn; 6, garnet edge: SMD 12, −93.00 to −93.09 m, wrigglite skarn; 7, garnet core: as 6 above; 8, garnet: SMD 5, −56 m, in calc-silicate skarn; 9, garnet: SMD 12, −92.00 to 92.12 m, upper calc-silicate skarn; 10, amphibole: SMD 12, −93.00 to 93.09 m, wrigglite skarn; 11, amphibole: SMD 12, −104.18 to −104.29 m, lower calc-silicate skarn; 12, amphibole: SMD 12, − 92.00 to −92.12 m, upper calc-silicate skarn; 13, annite: SMD 9, −97.2 m, sulfide-wrigglite skarn; 14, muscovite: SMD 16, −126.557 m, altered wrigglite skarn; 15, magnetite: SMD 12, −93.00 to −93.09 m, wrigglite skarn; 16, adularia: SMD 12, −39.00 to 93.09 m, wrigglite skarn.

TABLE 4. Composition of

The analyses were determined as described in Table 2 except that instead of being calculated as oxides they were calculated in terms

	1	2	3	4	5	6	7	8	9	10
Si	4.39	21.53	31.69	10.06	23.80	12.27	18.41	37.97	22.36	17.87
Ti	0.06	0.34	0.13	0.13	0.49	0.13	0.30	0.21	0.28	0.20
Al	1.08	5.48	2.38	4.68	7.56	4.73	6.46	1.58	4.25	4.08
Fe^{+3}	0.00	0.00	0.95	4.33	1.89	9.83	4.75	0.00	1.47	9.38
Fe^{+2}	0.63	1.95	2.88	14.55	3.68	6.34	2.64	1.76	6.23	0.06
Mn	0.05	0.02	0.12	0.12	0.62	0.59	0.85	0.10	0.30	0.05
Mg	0.95	1.39	2.61	1.14	1.75	1.15	1.39	2.05	5.09	1.88
Ca	36.83	13.41	7.00	18.20	11.70	22.95	20.80	4.34	13.51	21.68
Na	0.14	0.42	0.35	0.59	2.66	0.46	0.42	0.27	0.33	0.08
K	0.62	3.60	1.75	2.48	0.51	0.35	0.27	0.97	1.42	0.01
P	0.02	0.04	0.12	0.02	0.05	0.06	0.05	0.23	0.13	0.10
S	0.21	0.81	0.02	2.63	0.01	0.18	0.02	0.03	0.22	0.01
H^+	0.69	0.17	0.17	0.13	0.17	0.12	0.06	0.04	0.10	0.05
H^-	0.01	0.04	0.02	0.03	0.02	0.01	0.02	0.01	0.02	0.02
C	9.14	3.75	0.08	1.26	0.23	0.28	0.24	0.17	0.36	0.30
F	0	0.84 (?)	10.03	24.86	3.01	23.93	8.09	0.09	4.26	3.54
Total	54.82	53.79	60.30	85.21	58.05	83.38	64.77	49.82	68.33	61.11
wt. oxygen inferred (approx.)	45.18	46.21	39.70	14.79	41.95	16.62	35.23	50.18	32.67	48.89
Sr	344	272	38	97	188	36	34	50	100	11
Y	13 (40)	8 (60)	32 (100)	0 (60)	11 (60)	4 (70)	22 (50)	61 (100)	28 (70)	31 (60)
Pb	1	13	18	4	4	51	2	1	24	14
Th	4	15	8	123	15	148	15	10	67	16
U	0	1	1	5	1	5	1	1	1	2
Rb	20	102	591	791	217	42	60	158	233	6
Ga	3	14	10	44	19	24	20	4	17	13
Be	5	20	400	300	100	400	80	40	70	60
Sc	5	15	5	7	20	7	6	3	7	5
Mo	0	0	20	300	15	70	0	0	0	0
Yb	4	3	15	10	5	8	8	10	5	5
Sn	<20	<20	280	1,000	180	940	220	20	130	900
Li	5	25	100	65	25	30	15	20	50	5
Ci	0	0	99	35	0	1,799	230	32	116	750
Ni	28	45	77	112	111	62	65	42	100	79
Cu	20	27	7	869	36	289	25	16	66	26
Zn	0	28	89	67	131	173	82	45	334	129
W	<50	<50	2,400	2,100	130	500	190	<50	160	<50
B	0	50	3	0	3	300	0	3	5	150
Density	2.7382	2.6773	2.8479	3.6349	3.0090	3.5914	3.4473	2.8035	2.9698	3.5498

1, Gordon Limestone, field specimen from Iris River, CO_2 too high to do by the methods available; 2, siltstone interbed in Gordon Limestone (analysis 1); 3, SMD 5, −62 m, whole rock, fractured quartzite; 4, SMD 5, −46.5 m, whole rock, wrigglite skarn; 5, SMD5, −56 m, No. 1, green pyroxene-rich layer in calc-silicate rock, silty interbed in original limestone; 6, SMD 5, −56 m, No. 2, whole rock, calc-silicate, highly fractured + veins + green pyroxene-rich layer; 7, SMD 5, calc-silicate next to analyses 5 (free of veins and green pyroxene layer); 8, SMD 12, −111.36 to −111.46 m, pure quartzite whole rock; 9, SMD 12, −110.08 to −110.18 m, quartzite with vein-filled fractures, whole rock; 10, SMD 12, −106.02 to 106.13 m, calc-silicate rock, whole rock; 11, SMD 12, −104.18 to −104.29 m, calc-

correlation coefficients between the individual members from the two groups are usually negative (i.e., Zn:F = -0.13; Sn:Zn = -0.16) The two groups are believed to relate to the composition of the primary wrigglite skarn (group 1) and the later sulfide-rich alteration (group 2). These data imply that group 1 is removed by solution when sulfide (group 2) alteration occurs, as will be discussed. The distribution of W is erratic except for its correlation with Ge which may be accidental as only 13 pairs were analyzed. The W distribution is probably related to its irregular occurrence in veinlets (e.g., Fig. 4B). The Sc and Y correlations are erratic which may in part reflect the possible inaccuracy in the analysis (semiquantitative). Bi may have been redistributed during sulfide-amphibole alteration but not lost to solution as were the group 1 elements.

Table 7 shows the correlation coefficients of elemental concentrations as a function of depth in each drill hole. Those from group 1, namely Sn, F, and to

Quartzite, Skarn, and Limestone

of elemental abundances. The numbers in brackets are semiquantitative analyses by AMDEL.

11	12	13	14	15	16	17	18	19	20	21
12.63	8.68	10.40	16.67	5.13	12.19	3.06	16.78	7.67	10.79	5.06
0.16	0.06	0.08	0.28	0.07	0.13	0.05	0.37	0.14	0.11	0.08
4.55	5.49	5.21	5.18	1.34	5.10	0.64	5.45	2.56	5.01	1.41
9.50	2.48	2.85	5.33	0.17	1.65	0.18	3.57	0.00	4.16	0.09
5.87	18.26	16.80	1.53	2.08	11.75	1.36	2.14	1.30	13.45	1.34
0.88	0.35	0.54	1.48	0.23	0.60	0.21	0.98	0.02	0.50	0.14
1.13	0.86	0.92	1.74	1.42	1.80	1.40	2.92	1.47	1.17	1.31
22.79	18.26	18.66	23.46	36.58	21.88	36.90	21.66	33.11	19.96	35.86
0.30	0.30	0.18	0.01	0.10	0.38	0.01	0.04	0.15	0.35	0.10
0.46	1.31	1.57	0.02	0.22	0.76	0.12	0.03	1.26	1.32	0.56
0.06	0.02	0.03	0.04	0.02	0.03	0.03	0.06	0.03	0.03	0.03
0.01	1.96	2.48	0.01	0.15	1.95	0.10	0.04	0.37	1.81	0.21
0.12	0.35	0.22	0.06	0.00	0.22	0.02	0.13	0.02	0.21	0.18
0.02	0.03	0.03	0.01	0.04	0.03	0.06	0.04	0.04	0.03	0.03
0.15	0.64	0.66	0.38	9.53	1.23	10.18	1.06	8.44	0.79	9.32
24.05	23.25	22.32	13.78	0	21.84	0	3.31	0	23.26	0
82.68	81.20	81.94	69.98	47.08	81.54	54.32	58.58	56.56	82.95	55.72
17.32	17.70	17.05	30.02	42.92	18.46	45.68	41.42	43.44	17.05	44.28
21	61	57	21	279	109	225	16	361	69	302.3
13 (60)	0 (50)	0 (40)	20 (60)	9 (40)	0 (40)	13 (40)	16 (60)	12 (50)	3	12
20	0	0	6	2	0	0	6	0	5	1
64	238	298	37	4	190	7	27	7	183	5
3	8	2	2	1	4	1	2	1	4	1
32	605	699	4	37	84	28	7	58	442	31
20	33	32	14	4	26	4	16	7	31	4
300	400	300	200	70	400	30	100	5	340	28 (?)
7	4	3	30	3	4	3	15	7	5	4
0	70	5	0	0	60	0	0	0	87	0
5	5	3	4	2	2	3	4	3	5	3
950	660	780	200	100 (?)	620	30 (?)	310	<20	802	33 (?)
10	130	75	10	10	50	5	30	15	66	1
2,001	924	904	649	0	1,732	0	1,403	0	1,119	0
88	54	69	58	20	35	31	56	30	72	27
59	738	1,140	11	45	523	100	25	17	666	46
183	165	189	170	82	258	140	264	8	172	58
100	530	480	100	<50	240	<50	<50	<50	690	<50
200	40	50	150	3	200	0	600	3	98	1
3.5117	3.2988	3.4620	3.5368	2.8973	3.4285	2.8491	2.9431	2.7586	3.4672	2.8108

silicate rocks + wrigglite skarn, whole rock; 12, SMD 12, −99.13 to −99.20 m, wrigglite skarn, whole rock; 13, SMD 12, −97.5 to −97.59 m, wrigglite skarn, whole rock; 14, SMD 12, −96.19 to −96.28 m, calc-silicate rock, whole rock; 15, SMD 12, −93.00 to −93.09 m, unreplaced marble, whole rock; 16, SMD 12, −93.00 to −93.09 m, wrigglite skarn replacement of (15), whole rock; 17, SMD 12, −92.00 to −92.12 m, unreplaced marble, whole rock; 18, SMD 12, − 92.00 to −92.12 m, calc-silicate replacement of (17), whole rock; 19, SMD 12, −83.32 to −83.48 m marble, whole rock; 20, average wrigglite skarn (this table); 21, average marble (this table).

a lesser extent Be, show a decreasing concentration trend with depth in traverse 1 but not traverse 2. The values from group 2, namely Mo, Cu, and Zn, are erratic throughout. This is interpreted to show that the sulfide-rich replacement, particularly common near the Bismuth Creek fault, is somewhat erratic and selective, relating to permeability present after the primary skarn crystallization.

In traverse 1, the average value of the concentration for each drill hole of the group 1 elements (F, Sn, and Be) as well as W, Mo, and Bi is approximately constant relative to their proximity to the Bismuth Creek fault. Cu shows a decrease while Zn shows an almost three-fold increase toward the fault. In traverse 2, where there are only three values per element, Zn increases to the west while Sn, F, Be, and Mo decrease. The data suggests that Zn is derived from the Bismuth Creek fault whereas the group 1 elements were derived from a more extensive plumbing system (east-west fracture systems incorporating

TABLE 5. Differences of Composition between Rocks and Their Unreplaced Equivalents

The values are in terms of molar differences per 100 cm^3 of rock analyzed. The molar values were calculated from Tables 2 and 4 using the density data.

	1	2	3	4	5	6	7	8	9	10	11	12
Si	0.0073	−0.4074	−0.0229	0.6639	−1.4261	−0.5768	2.7273	0.4974	0.8256	0.9587	1.4479	−7.5205
Ti	−0.0002	0.0007	0	−0.0039	0.0049	−0.0065	0.0170	0.0117	0.0032	0.0050	0.0199	−0.1105
Al	−0.0006	0.0891	0.0028	−0.1230	0.3034	0.0869	0.6806	0.2993	0.4969	0.5040	0.5270	−6.8172
Fe^{+3}	−0.0007	0.0089	0.0033	−0.0440	0.0077	0.0048	0.2924	0.1017	0.2577	0.0924	0.1790	−2.7357
Fe^{+2}	0.0903	0.0921	0.0106	−0.3699	−0.0102	0.0586	0.0967	0.1049	0.7674	0.6136	0.0435	−6.0764
Fe^{total}	0.0910	0.1010	0.0139	−0.4139	−0.0025	0.0634	0.3891	0.2066	1.0251	0.7060	0.2225	−8.8121
Mn	0.0027	0.0044	0.0012	−0.0223	0.0113	0.0013	0.0465	0.0329	0.0246	0.0251	0.0416	−0.4025
Mg	0.0016	0.0060	0.0019	−0.0298	0.3856	−0.2223	0.0480	0.0636	0.0153	0.0845	0.1894	−1.7957
Ca	0.0049	0.0516	−0.0022	−0.0867	0.6975	0.1939	−0.6870	−0.0175	−0.7881	−0.7728	−1.0327	5.4418
Na	−0.0650	−0.0599	−0.0522	1.7911	0.0100	0.0105	0.0512	0.2992	0.0406	0.0421	0.0039	−1.1623
K	−0.0097	0.0434	−0.0034	0.0083	1.0091	0.0581	−0.0158	0.2075	0.0770	0.0503	−0.0064	−4.4106
P	0	0	0.0001	−0.0011	−0.0082	−0.0096	0.0027	0.0013	0.0007	0.0017	0.0028	0.0125
S	0.0706	0.0209	0.0048	−0.1977	0.0018	−0.0008	−0.0159	−0.0668	0.1777	0.1948	−0.0053	−1.0659
H^+	0.0054	0.0101	0.0036	−0.0191	0.1849	0.3720	−0.2914	0.0564	0.2222	0.7543	0.3257	−1.5751
C	0.0351	0.0097	0.0038	−0.0592	0.0493	−0.0207	−2.0787	−0.7784	−1.9531	0.3415	−2.1550	20.9970
F	−0.0098	0.3569	0.0049	−0.4256	0.6526	1.4905	1.4679	0.3583	4.2445	3.9411	0.5127	−36.841

1, average of zone 4, average of zone 1, Table 2

2, average of zone 4, average of zone 2, Table 2

3, average of zone 4, average of zone 3, Table 2

4, molar gains and losses by the solution for the greisenized section; values are in moles/100 cm^3-meters; intersections of zones used are: zone 1, 1.75 m; zone 2, 1.05 m; zone 3, 10.87 m; and zone 4, 21.49 m

5, replacement of quartzite: veined quartzite (9, Table 4), pure quartzite (8, Table 4)

6, replacement of veined quartzite (3, Table 4), pure quartzite (8, Table 4); veined quartzite is shown in Figure 4A

7, replacement of silty sediment pyroxene skarn (5, Table 4), siltstone (2, table 4); pyroxene skarn is shown in Figure 4B

8, replacement of marble; calc-silicate skarn (7, Table 4), average marble (21, Table 4); calc-silicate skarn is shown in Figure 4B

9, replacement of marble; wrigglite skarn (20, Table 4), unreplaced average marble (21, Table 4)

10, replacement of marble; wrigglite skarn (16, Table 4), unreplaced adjacent marble (15, Table 4); see figure 5C for relation

11, replacement of marble; calc-silicate skarn (18, Table 4), unreplaced adjacent marble (17, Table 4); see Figure 4E for relation

12, molar proportions of elements lost to and gained from solutions while traversing and reacting in section (SMD 12); values are in moles/100 cm^3 m; thicknesses are: veined quartzite, 3.31 m; lower calc-silicate unit, 3.81 m; laminar skarn, 7.40 m; and upper calc-silicate unit, 0.97 m

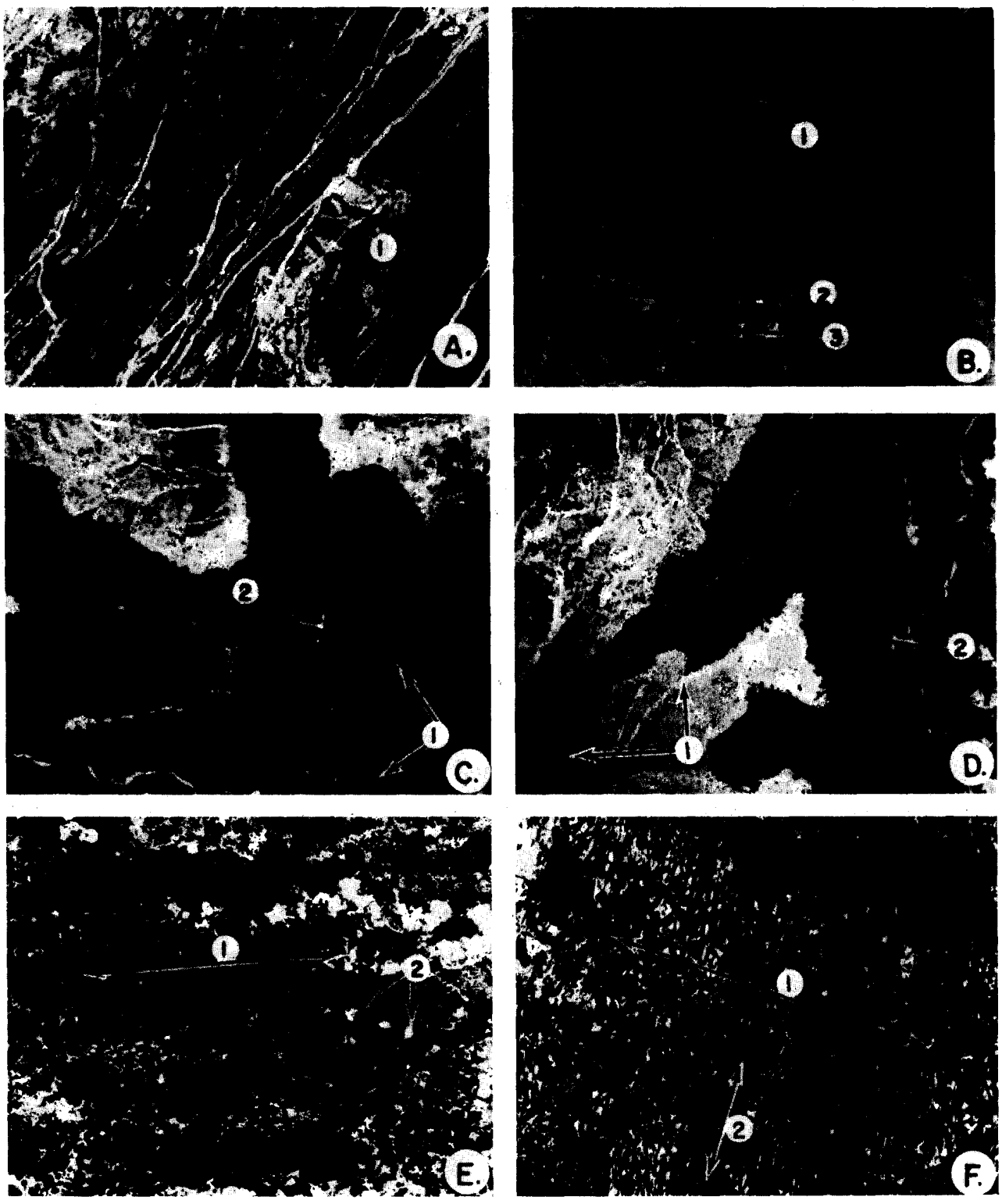

FIG. 5. Features of primary wrigglite skarn and secondary sulfide replacement.

A. SMD 5, -56 m, shows the extremely fractured "sheeted" appearance of wrigglite skarn and garnet skarn common near the skarn-quartzite contact. (1) shows a mineral-filled fracture. The field of view is 4 cm wide.

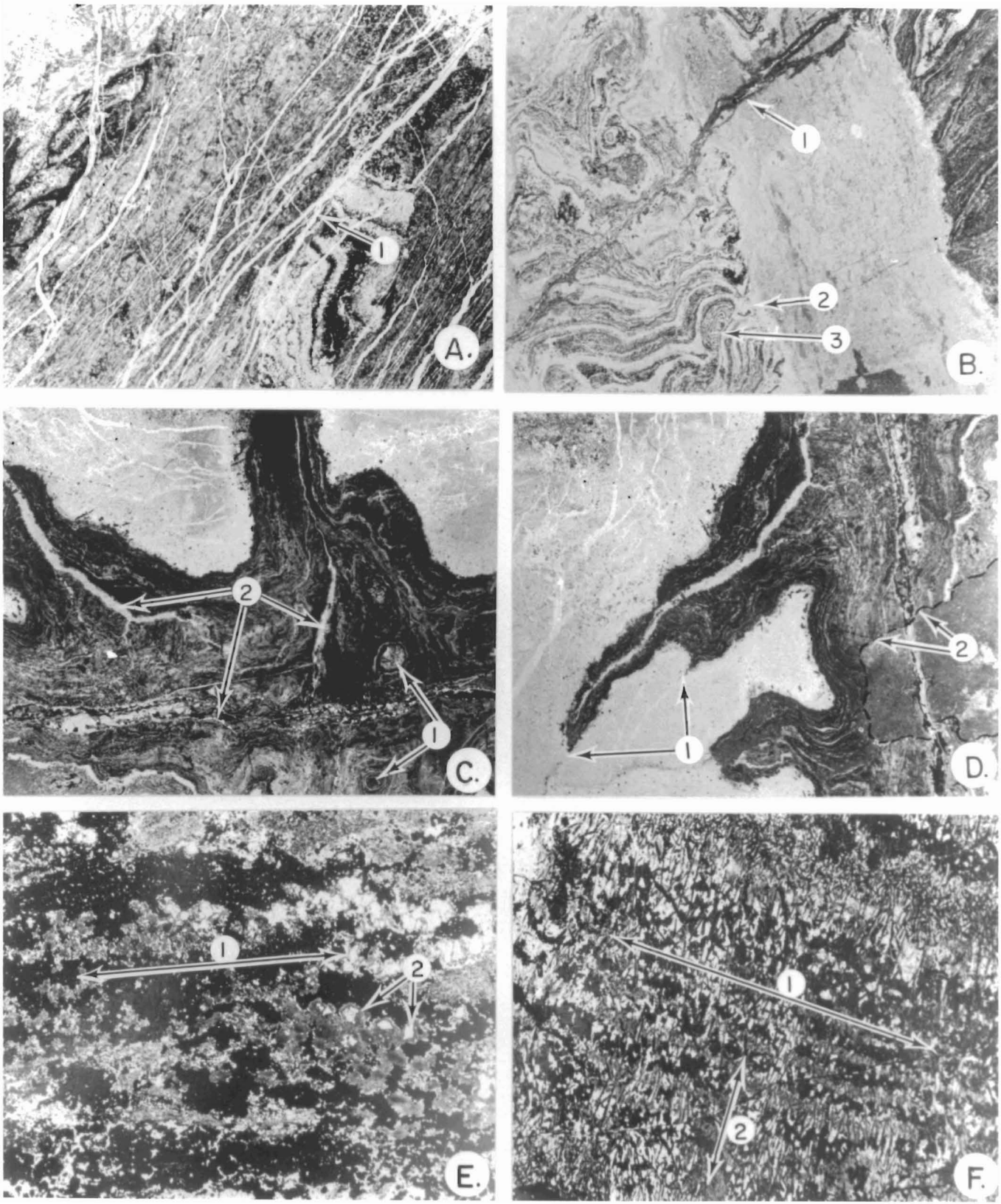
1
A.
1
2
3
B.
2
1
C.
2
1
D.
1
2
E.
1
2
F.

the quartz lodes?). This is consistent with the Bismuth Creek fault being active after as well as during wrigglite skarn deposition.

The Occurrence of Elements of Economic Importance in the Skarns

At Moina, Sn occurs in a number of ways, namely, in solid solution in garnet (to 0.70 wt %), in Sn sphene, and as cassiterite. AMDEL (1978) regarded the tin content partly as a solid solution in garnet (45%) and also as cassiterite of very fine grain size (55%). Green (1979) has shown that at Moina, cassiterite occurs as laminar inclusions of 1.5 to 5 μm long in garnet. These were not found by the present authors although cassiterite grains to 15 μm in size were observed in the magnetite-rich layers in the wrigglite skarn. No distinct Be mineral such as helvite was found and Be is presumed to occur in vesuvianite. Beus (1966, p. 144) found Be values in vesuvianite up to 9.20 weight percent and in garnet, 0.39. W is in scheelite in the skarn fabric and in wolframite plus scheelite in veins; no significant values of W in any of the other minerals was found. F is mainly in fluorite (>90%) with topaz + F-micas in veins; similarly, Bi is in bismuthinite, Mo in molybdenite, Cu in chalcopyrite, and Cd and In in sphalerite. Au may occur as a solid solution in bismuthinite, as the correlation data suggest, or simply as free gold.

Fluid Inclusions

Primary fluid inclusions in the skarn minerals were not found, reflecting their fine-grained nature, whereas measureable inclusions occur only sparingly in vein minerals. Fluid inclusions should represent those present during skarn genesis because the mineralogy of the veins is similar to that of the skarn; the intersecting nature of successive periods of vein deposition suggests cogenesis (Fig. 3). In quartz (SMD 12 at 155 m), liquid CO_2 is a common but not constant constituent (Fig. 8B, E, and F). The daughter products are NaCl (D_1) and fluorite (D_2) as confirmed by SEM analyses, with a rare reddish opaque which is possibly hematite (Fig. 8D) and a number of minute grains of unidentified nonopaque daughter products. Homogenization temperatures were 331° ± 12°C (average of 12; gas dissolved into the liquid phase in seven cases and liquid into gas in five). This variation, together with the fact that gas-rich and saline liquid-rich inclusions occur together (Fig. 8H), suggests the inclusions were trapped from a boiling solution. NaCl dissolved before the homogenization temperature was reached while CaF_2 did not, perhaps due to slow kinetics. The first melting of previously frozen inclusions gave temperatures of −23.1° ± 0.4°C (average of six) and the last melting of ice, −15.3° ± 2.2°C (average of six).

Fluid inclusions in fluorite in a fluorite-rich vein (SMD 16 at 43.9 m depth) contain no liquid CO_2. Homogenization temperatures of the commonly five-phase inclusions are 482.8° ± 9.2°C (average of eight; three homogenized into gas, five into liquid), with a first melting temperature of −19.5° ± 3.0°C (average of eight) and a last melting of −7.0° ± 1.5°C (average of eight). Fluid inclusions in topaz in a cassiterite-wolframite-bismuthinite quartz vein (stratigraphically below the skarn, reference points 1700E, 100S, Fig. 1A) contained no liquid CO_2 and generally two daughter products (Fig. 8G). Homogenization was at 416° ± 5.2°C (average of 10; eight dissolved into liquid, two into gas), with a first melting temperature of −15.0° ± 1.5°C (average of seven) and a last melting of −6.4° ± 0.8°C (average of seven). The pressure correction for the homogenization temperatures is unknown but is probably small as the deposit was likely formed at near-surface conditions.

On the basis of the limited data available, the following conclusions are drawn: the homogenization of fluid inclusions constituents into both the liquid and the gas phase, with the large variation of ratios ob-

B. SMD 12, -101.28 m, showing the interface (2) between wrigglite and pyroxene skarn. (3) shows a concentrically zoned wrigglite skarn area. (1) shows a fluorite-rich fracture which obviously has altered pyroxene skarn to a greater extent than wrigglite skarn. Field of view is 2 cm wide.

C. SMD 12, -80 m; wrigglite skarn replacement of marble. The central fractures (2) have been filled in by a variety of vein materials. (1) refers to augen-type features near the intersection of major fractures. Field of view is 3 cm wide.

D. SMD 12, -80 m, wrigglite skarn replacement of marble showing the parallel relationship between the original fracture and the lamination of the skarn. (2) shows the interface between amphibole-sulfide replacement area and unreplaced wrigglite skarn. Field of view 3 cm wide.

E. SMD 16, -65 m, transmitted light photomicrograph of layered sphalerite base metal sulfide skarn after garnet or wrigglite skarn. The lamination is parallel to (1). (2) shows garnet partly altered to hematite quartz. Field of view is 1 cm wide.

F. SMD 9, -97.2 m, transmitted light photomicrograph of pyrrhotite replacement of primary laminar skarn. Relict wrigglite skarn lamination is parallel to (1) whereas a later superimposed fabric is shown by (2). Field of view is 1 cm wide.

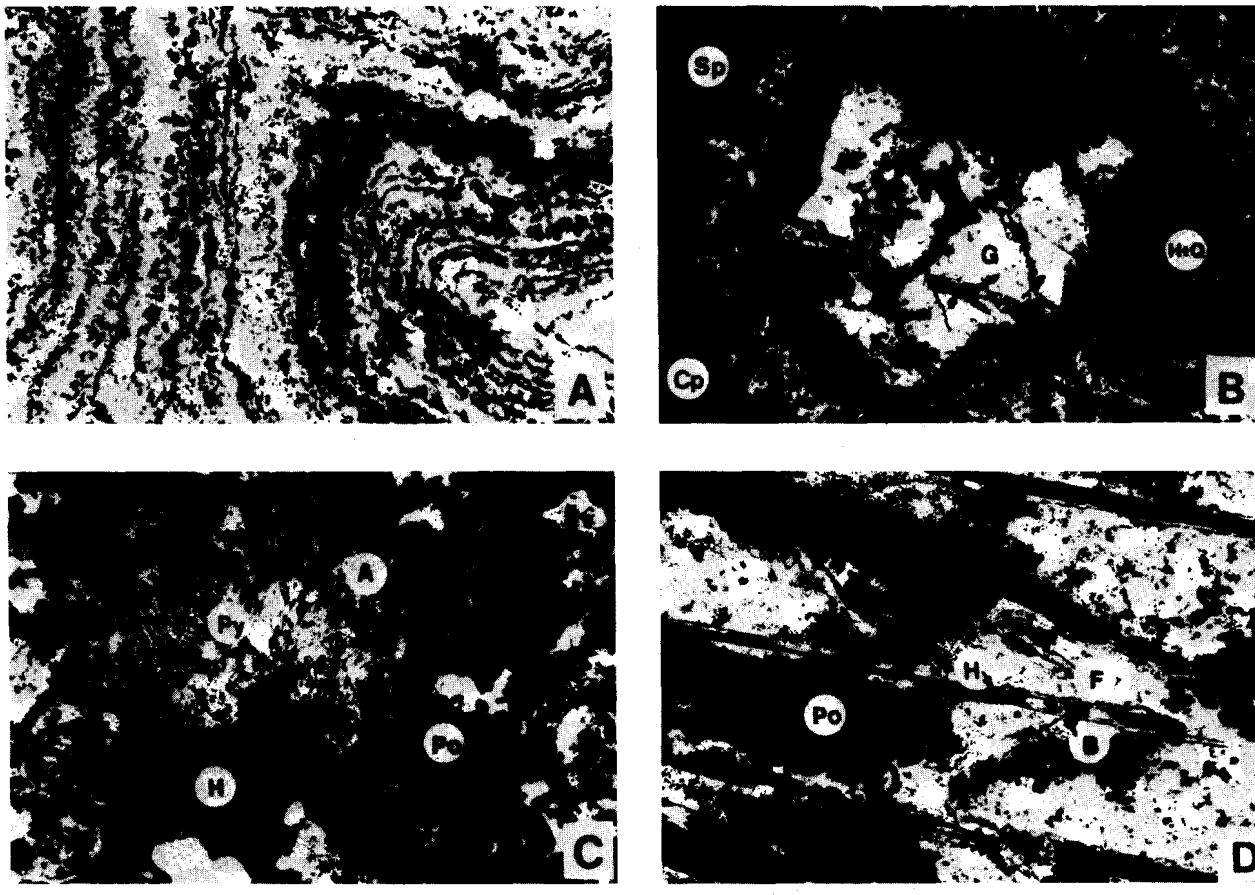

FIG. 6. Textures in primary wrigglite skarn and replacement of this skarn.

A. Typical wrigglite skarn showing that the dark (magnetite ± cassiterite) lamellae are not continuous. The apparent foldlike form is due to irregularities in permeability (see text for explanation); SMD 5, -46.5 m. Field of view is 0.9 cm wide.

B. Replacement of garnet (G) by hematite + quartz (H + Q) with sphalerite (Sp) and chalcopyrite (Cp). Enlargement of replacement feature in Figure 5E; SMD 16, -65 m. Field of view is approximately 1 mm wide.

C. Replacement of pyroxene (Py) by amphibole (A) with associated hematite (H) and pyrrhotite (Po). Field of view is approximately 1.1 mm wide; SMD 16, -65 m. Some of the light areas are fluorite.

D. Replacement of wrigglite skarn by pyrrhotite (Po) with fluorite (F) retained. Enlargement of a part of Figure 5F, SMD 9, -97.2 m. A later fabric consisting of hematite plates (H) with marginal F annite (B) has been superimposed upon the already replaced laminar skarn. This suggests hematite is a postsulfide replacement. Field of view is approximately 1 cm wide.

served, implies that boiling the hydrothermal solutions occurred at some time during genesis, and salinities were high (≃30–40 equiv. wt % NaCl). The major constituents in the fluid phase are NaCl, (KCl?), H_2O, and CO_2. Some CaF_2 occurs either as a daughter product or as accidental crystals. The first melting temperatures near −20°C confirm that NaCl (+KCl?) is the major salt present and that $CaCl_2$ is not present. Systems involving the latter salt show first melting temperatures near −52°C (the ternary eutectic in the system $CaCl_2$-NaCl-H_2O).

Sulfur Isotopes

Table 8 shows sulfur isotope values from the Moina area done by Dr. Shen-Su Sun of the Division of Mineralogy, CSIRO. These values are relative to the Cañyon Diablo standard and the analytical uncertainity is believed to be better than 0.2 per mil. As can be seen sulfides from wrigglite, pyrrhotite-rich (amphibole), pyrite-rich (amphibole), and sphalerite-rich skarns have similar sulfur isotopic values (8.4 to 9.3‰) to those of pyrite in the greisenized granite

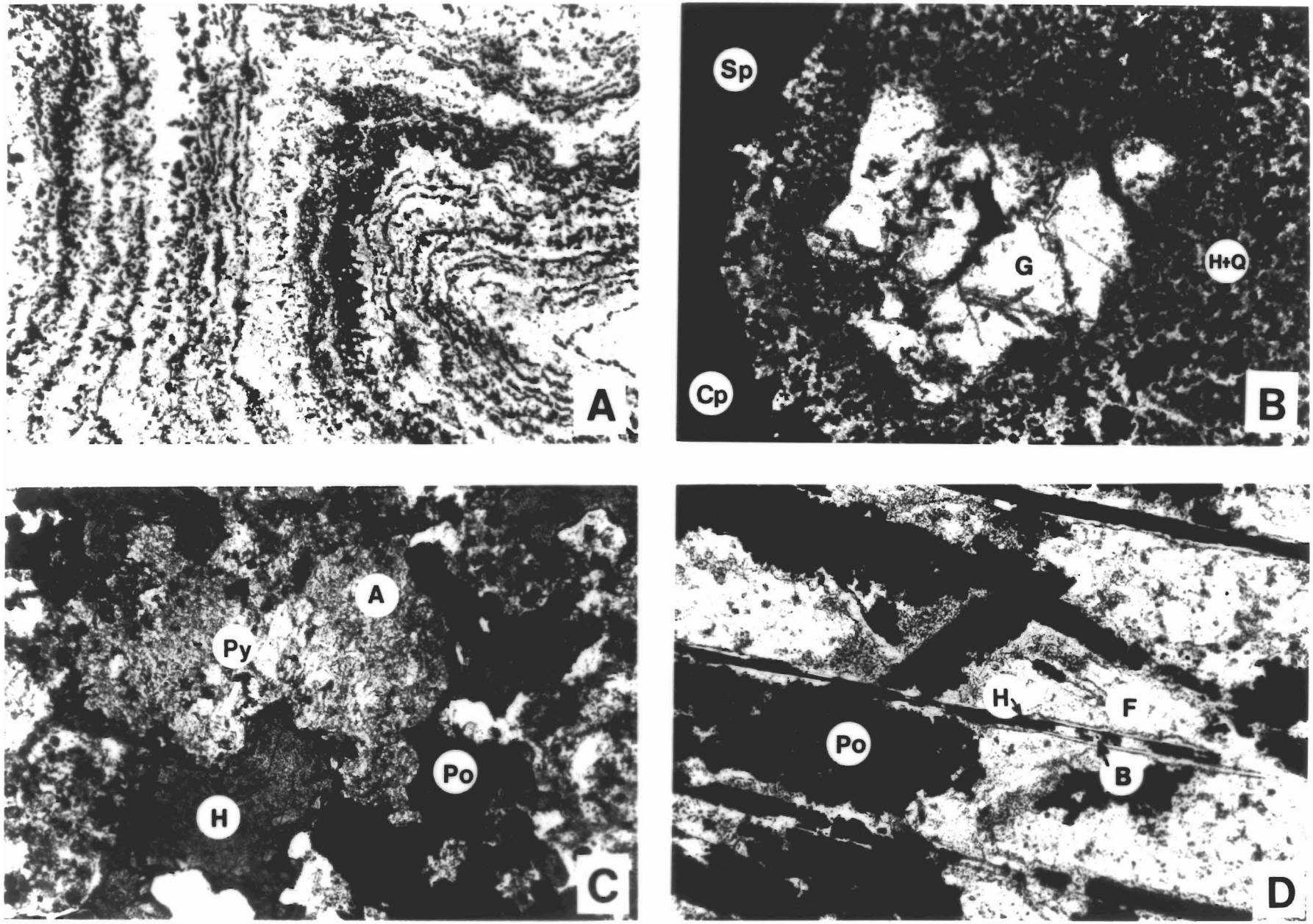
A
Sp
G
H+Q
Cp
B
A
Py
Po
H
C
H
F
Po
B
D

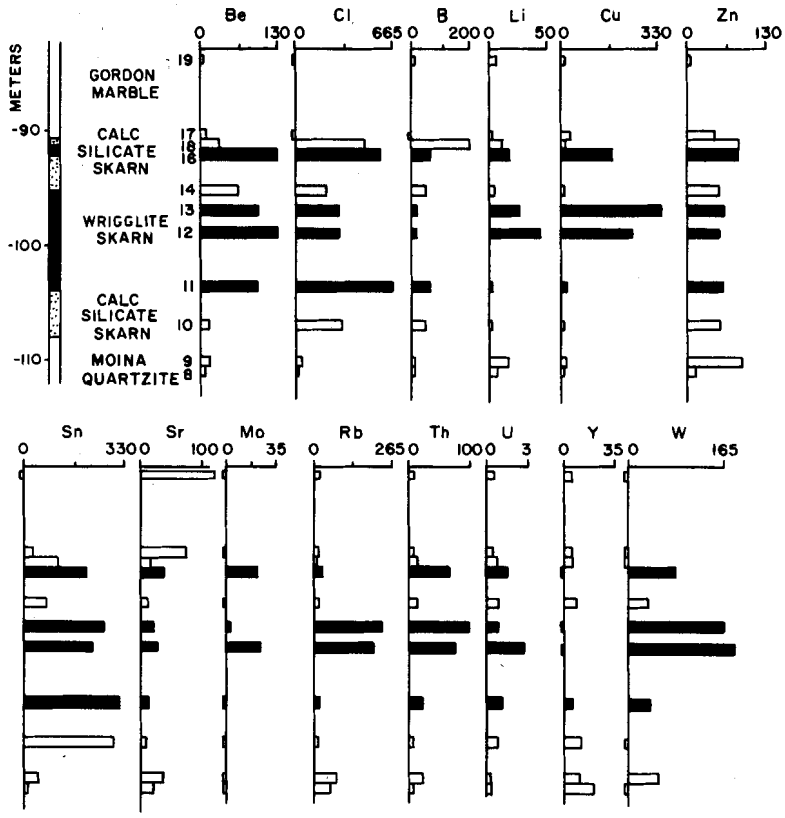

FIG. 7. Histograms of chemical variations through the quartzite-skarn-limestone section of SMD 12 (see Fig. 1A for location). The numbers 8 to 19 refer to the analyses in Table 4. The values are in moles per 100 cm^3 of rock (to account for density differences). The dark bars to the right of the vertical line refer to wrigglite skarn composition values. Values shown to the left of the vertical line indicate that the analysis yielded no values of the element.

(8.9‰). Pyrrhotite from SMD 14 (at 38 m depth below the collar) limestone and framboidal pyrite from the Moina sandstone have negative values (−4.2 and −6.9‰, respectively). Pyrite from metasomatized sandstone (SMD 18 at 102.5 m depth) and pyrite and pyrhotite from the margin of the skarn (Moina) have intermediate values (≃4.5‰).

Sulfur isotope $\delta^{34}S$ values of hydrothermal fluid can be as much as 4 per mil larger that the $\delta^{34}S$ melt if the volume ratio fluid to melt is small (Ohmoto and Rye, 1979, p. 527). Average $\delta^{34}S$ values of silicic igneous rocks of as high as 10 ± 5 per mil have been suggested (Holser and Kaplan, 1966), and individual values as high as 30 per mil have been recorded (Shima et al., 1963). Presently accepted values, however, are approximately 0 ± 3 per mil (Ohmoto and Rye, 1979, p. 524).

The greisenized granite and skarn values (≃9‰) have a sulfur source which is quite constant but is unlikely to be purely magmatic in origin. Coexisting pyrrhotite-pyrite pairs in SMD 9 (−102.50 m) and Moina 13 have similar values. On the basis of sulfur fractionation thermometers (Ohmoto and Rye, 1979, p. 518), this would suggest they crystallized at very high temperatures (>700°C), which is geologically unlikely, or they did not coexist stably (not formed at the same time). The latter explanation is most likely on textural evidence. Sulfur isotope values are known for the Renison Bell Sn replacement body (Patterson and Ohmoto, 1976). Here, $\delta^{34}S$ values of pyrrhotite in the ores are near 6.5 per mil and the primary (?) sulfide in the associated granite have $\delta^{34}S$ values near 3.5 per mil. Patterson and Ohmoto (1976) interpreted this to mean the sulfur has a magmatic source.

Discussion

Origin of wrigglite skarn at Moina and elsewhere

Fluorite-rich wrigglite skarns are known from many other localities including: Dragoon Mountains,

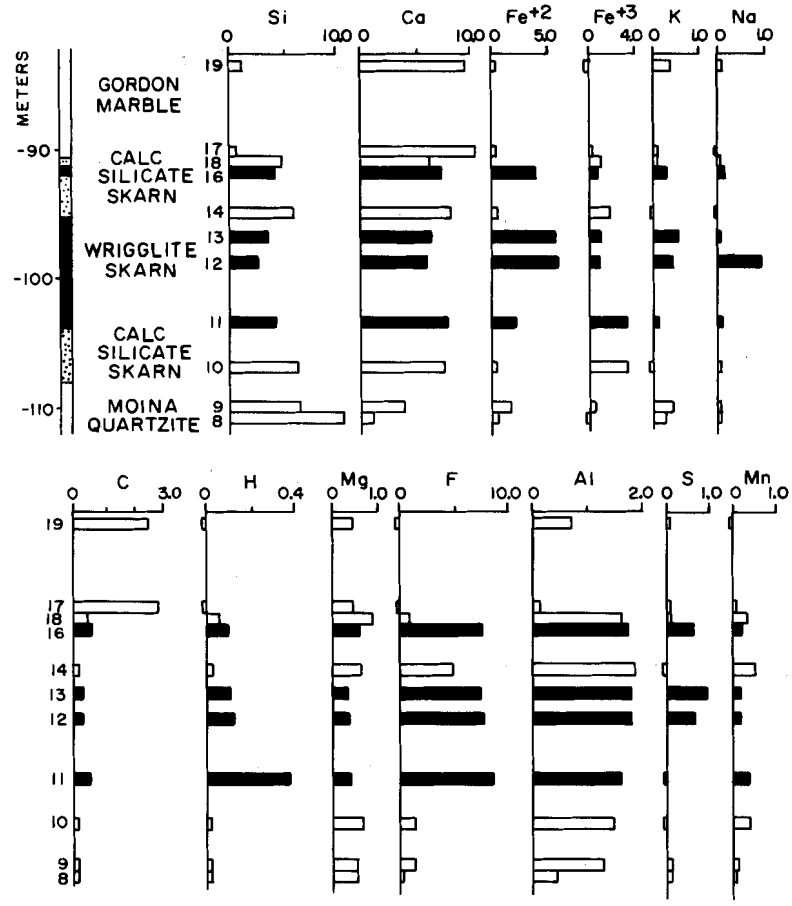

FIG. 7 (cont.).

Arizona, (Perry, 1964); Iron Mountain, New Mexico (Jahns, 1944b); Lost River, Alaska (Knopf, 1908; Sainsbury, 1964, 1969); south China (Meng, 1937; Hsieh, 1963; Beus, 1966); Chugako, Japan (Miyake, 1965); Kazakhstan, USSR (Beus, 1966; Zasedatelev, 1973; Ermilova and Senderova, 1959); Iten' Yrginsk, Chukotka, USSR (Shcherba, 1970; Getmanskaya, 1972); various other deposits in the Far Eastern Province, USSR (Govorov, 1958); Dal'negorsk, Primor'ye, USSR (Aleksandrov, 1975); Kristiana, Norway (Twelvetrees, 1913); Mt. Garnet, Queenland (Askins, 1976); and Mt. Bischoff, Tasmania (observed by one of us—P.W.A.). They are related to leucogranite plutons or dikes exhibiting greisenization and are usually found in Paleozoic limestone terrains (Govorov, 1968). There is invariably intense fracturing and faulting and, at least in some cases, boiling of the hydrothermal solutions can be demonstrated (evidence from the study of W. Brown at Mt. Garnet, pers. commun., 1979; at Moina and Mt. Bischoff, P. Collins, pers. commun., 1979). The primary skarn is enriched in F, Fe, Sn, W, Be, Li, B, and Bi whereas secondary alteration commonly produces skarn rich in Zn, S, Pb, and Cu (e.g., at Mt. Garnet, Askins, 1976; Dal'negorsk, Aleksandrov, 1975; and at Moina). Anomalously high values of such elements as B, In, Cd, and Li may occur (Sainsbury, 1969).

Bulk chemical analyses of wrigglite skarn by Zasedatelev (1973), Miroshnchenko and Gulyayev (1978), Waite (1978); Sainsbury (1969), and the present authors indicate that when the fluorine content is less than about 9 weight percent the wrigglite structure does not form and granular skarn forms instead. In a cuspidine wrigglite skarn from Mt. Garnet (Askins, 1976), the lamination is indistinct and F $\simeq$ 9.0 weight percent.

Wrigglite skarn is fine grained, has a contorted structure, and is commonly associated with coarser grained, F-poor, granular skarn. Individual lamellae, which contain restricted mineral assemblages, pinch and swell and may contain crosscutting septalike veinlets of magnetite (at Moina) or tourmaline (at

TABLE 6. Correlation Coefficients of Elemental Abundances of Elements Relative to Others

	Pb	W	Bi	Sn	Mo	Cu	Zn	Be	F	Sc	Y	Cd	In	Ge	Au	Ag
Pb		−0.22	0.27	−0.11	0.09	0.30	0.41	−0.20	−0.21	−0.02	−0.24	0.21	0.34	0.26	0.56	−0.12
W	262		0.13	0.00	0.06	0.14	−0.01	0.18	0.15	0.03	−0.00	−0.35	−0.13	0.58	−0.01	−0.32
Bi	263	344		0.08	−0.11	0.30	0.28	0.13	0.15	−0.09	−0.27	0.33	0.47	0.49	0.80	0.25
Sn	285	401	364		0.59	−0.05	−0.16	0.32	0.20	−0.49	−0.56	−0.06	0.06	0.16	−0.18	−0.03
Mo	229	313	305	321		−0.05	−0.05	0.06	−0.03	0.07	0.08	−0.63	−0.30	0.39	−0.12	−0.24
Cu	278	265	260	282	228		0.62	−0.09	−0.06	−0.11	−0.16	0.77	0.54	−0.05	0.45	0.22
Zn	290	324	324	347	284	287		−0.22	−0.13	−0.05	−0.09	0.99	0.74	0.04	0.71	0.01
Be	284	359	358	382	316	281	346		0.26	−0.11	−0.11	0.06	−0.04	0.40	−0.26	0.39
F	287	364	364	387	321	284	349	384		−0.46	−0.47	−0.41	−0.16	0.33	−0.24	0.44
Sc	56	130	132	145	109	57	109	50	148		0.71	−0.14	−0.00	0.41	−0.13	0.00
Y	56	125	127	140	104	57	105	145	143	144		−0.00	−0.03	0.10	−0.34	0.00
Cd	20	8	18	20	6	20	20	20	20	20	20		0.74	−0.05	0.46	0.00
In	41	25	33	40	16	42	42	42	41	42	42	18		0.25	0.39	0.00
Ge	19	13	17	19	8	19	19	19	19	19	19	8	15		0.17	−0.15
Au	93	80	85	96	73	90	96	90	96	46	46	18	35	18		
Ag	25	20	24	25	23	17	25	19	24	0	0	0	0	0	20	

The upper right hand part of the table gives the correlation coefficients between elements and the lower left hand part gives the number of pairs used. When the concentration of an element was zero, the value was not used for correlation. The program used was written by Ms. Judy Hannah of the Department of Geology, University of California, Davis, California. The program fits the data to a linear function and calculates correlation coefficients.

TABLE 7. Correlation Coefficients of Elemental Abundance of Economically Important Elements in Weight Percent vs. Depth in the Skarn Profile

Also given are the range of values and the average value for each drill hole. All rock types that contain mineralization are included, of which wrigglite skarn predominates.

Traverse 1	W	Bi	Sn	Mo	Cu	Zn	Be	F
DDH 4 (32 analyses each)								
Cor. coef.	−0.214	−0.678	−0.755	−.026	−0.249	−0.362	−0.650	−0.751
Range	70–2,220	0–780	30–2,100	0–150	5.350	18–1,240	70–700	0.63–12.89
Average	744	305	1,178	43	117	130	266	5.86
DDH 11 (42 analyses each)								
Cor. coef.	0.162	−0.678	−0.357	0.301	0.165	−0.027	−0.411	−0.535
Range	50–6,500	8–820	620–2,950	0–370	10–350	30–450	70–500	2.91–12.41
Average	1,040	402	1,490	50	120	116	252	7.98
DDH 6 (70 analyses each)								
Cor. coef.	−0.073	−0.266	−0.372	0.380	−0.234	0.133	−0.036	−0.587
Range	55–4,600	0–2,100	46–5,000	0–360	5–190	45–4,550	70–600	1.51–14.60
Average	879	430	1,302	62	45	216	2.44	7.74
DDH 15 (41 analyses each)								
Cor. coef.	0.171	−0.680	−0.672	0.355	ND	ND	−0.391	−0.699
Range	45–3,650	0–700	60–3,600	0–150	ND	ND	80–500	0.73–12.41
Average	1,092	403	1,321	43	ND	ND	256	7.88
DDH 7 (60 analyses each)								
Cor. coef.	−0.193	−0.305	−0.780	0.104	−0.232	−0.200	−0.264	−0.268
Range	95–3,400	0–2,050	180–2,750	0–290	2–440	55–9,800	80–300	1.31–14.07
Average	878	391	1,169	47	46	366	200	8.17
Traverse 2								
DDG ML-3 (38 analyses each)								
Cor. coef.	0.307	0.364	−0.481	−0.209	−0.078	0.000	−0.532	−0.432
Range	0–1,400	0–1,060	1–8,200	0–2,075	0—910	10–435	1–370	0–15.00
Average	317	259	2,223	245	64	147	180	6.69
DDH 16 (53 analyses each)								
Cor. coef.	−0.018	0.049	−0.059	0.052	ND	−0.096	0.292	0.120
Range	15–6,500	20–2,000	190–2,650	0–200	ND	55–154,000	50–5,000	0.34–12.05
Average	728	416	933	42	ND	11,852	160	5.14
DDH 13 (57 analyses each)								
Cor. coef.	0.213	−0.180	−0.361	0.434	−0.228	−0.082	0.312	0.244
Range	0–1,850	0–2,100	8–720	0–34	2–910	42–275,000	2–1,000	0.01–5.60
Average	69	266	299	9	151	24,182	81	0.60

The samples represent analyses of split core of 1 m length, in most cases. The positions of the drill holes are shown in Figure 1A. W, Bi, Sn, Mo, Cu, Zn, and Be are in terms of ppm while F is in terms of weight percent. Values of Pb, Sc, Y, Cd, In, Ge, Au, and Ag are not included because they are only minor constituents of the skarn. Their ranges in ppm are Pb (0–110), Sc (0–20), Y (0–70), Cd (0–1340), In (0–90), Ge (0–5), Au (0–4.5), and Ag (0–2).

Lost River). The following mineral assemblages, occurring in the alternating dark and light lamellae, respectively, were observed by the authors in skarn(s) from different areas: (a) magnetite ± cassiterite: vesuvianite + fluorite (most common); (b) magnetite + cassiterite: adularia + vesuvianite + fluorite (rare, Moina); (c) magnetite ± cassiterite: hedenbergite + fluorite ± andradite (rare, Moina); (d) f annite + magnetite: fluorite (rare Mt. Garnet); (e) magnetite rimmed by gahnite: f cuspidine + vesuvianite + fluorite (rare, Mt. Garnet); (f) pyrrhotite + cassiterite ± stannite: F biotite + F-Na tourmaline + fluorite + sellaite (rare, Mt. Bischoff); and (g) chrysoberyl + F margarite + F-Na tourmaline: fluorite + F margarite (Lost River).

Other common minerals are: helvite, danalite, hematite, spinel, lithian mica, and Ca-rich plagioclase (Govorov, 1968; Shabynin, 1977). Wrigglite-like skarn consisting of alternating magnetite and garnet has been recorded from the Kearney mine, Hanover, New Mexico (D. M. Burt, pers. comm., 1979).

Different authors believe that wrigglite skarns rep-

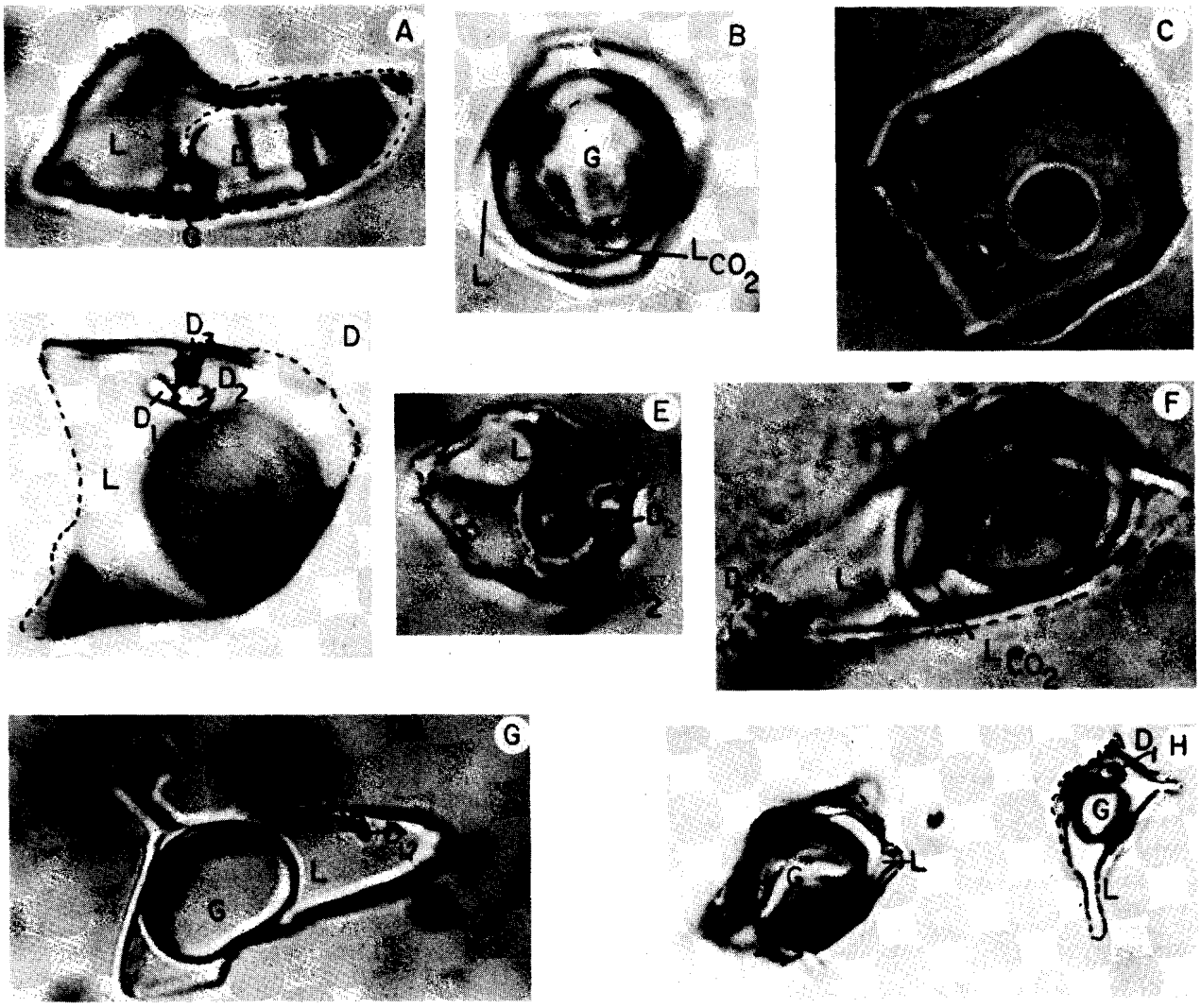

FIG. 8. Fluid inclusions in minerals associated with the wrigglite skarn. A, B, C, D, E, F, and H are from a quartz (-cassiterite-fluorite) vein in SMD 12 at 155 m. Note the liquid CO_2 (L_{CO_2}) daughter products (D), gas (G), and liquid (L). D_1 = NaCl, D_2 = fluorite, and D_3 = probably hematite. The coexisting gas-rich and liquid-rich fluid inclusions (H) have been interpreted to indicate that boiling occurred during trapping. G shows a highly saline fluid inclusion in topaz (described in text). All the fluid inclusions are generally 15 to 30 microns wide.

resent: (1) bedding in an unusual sediment (Zasedatelev, 1973), (2) replacement of fine bedding and/or stromatolites (P. W. Stainton, pers. commun.,), (3) colloform, solidified gel precipitates (as in Stevenson and Jeffery, 1964), (4) rhythmical deposition in cavities (Trustedt, 1907), and (5) deposition by replacement at diffusion fronts moving outward from fractures (Knopf, 1908; Jahns, 1944a; Eskola, 1951; Beus, 1966; Sainsbury, 1969; Georgievskaya, 1955; Shabynin, 1977).

In Zasedatelev's model, wrigglite skarn is formed as chemical sediment in small, strongly evaporated basins, the unusual components (F, Be, Sn, W, etc.) being attributed to thermal springs of volcanic association. The rhythmic layering is a possible seasonal effect and chemical deposition is a colloidal precipitate producing colloformlike textures. Diagenesis, regional metamorphism, and finally contact metamorphism by a granite caused recrystallization of the sediment to its present mineralogical composition. The evidence against such an origin is strong. The laminations consist of folded, commonly pipelike

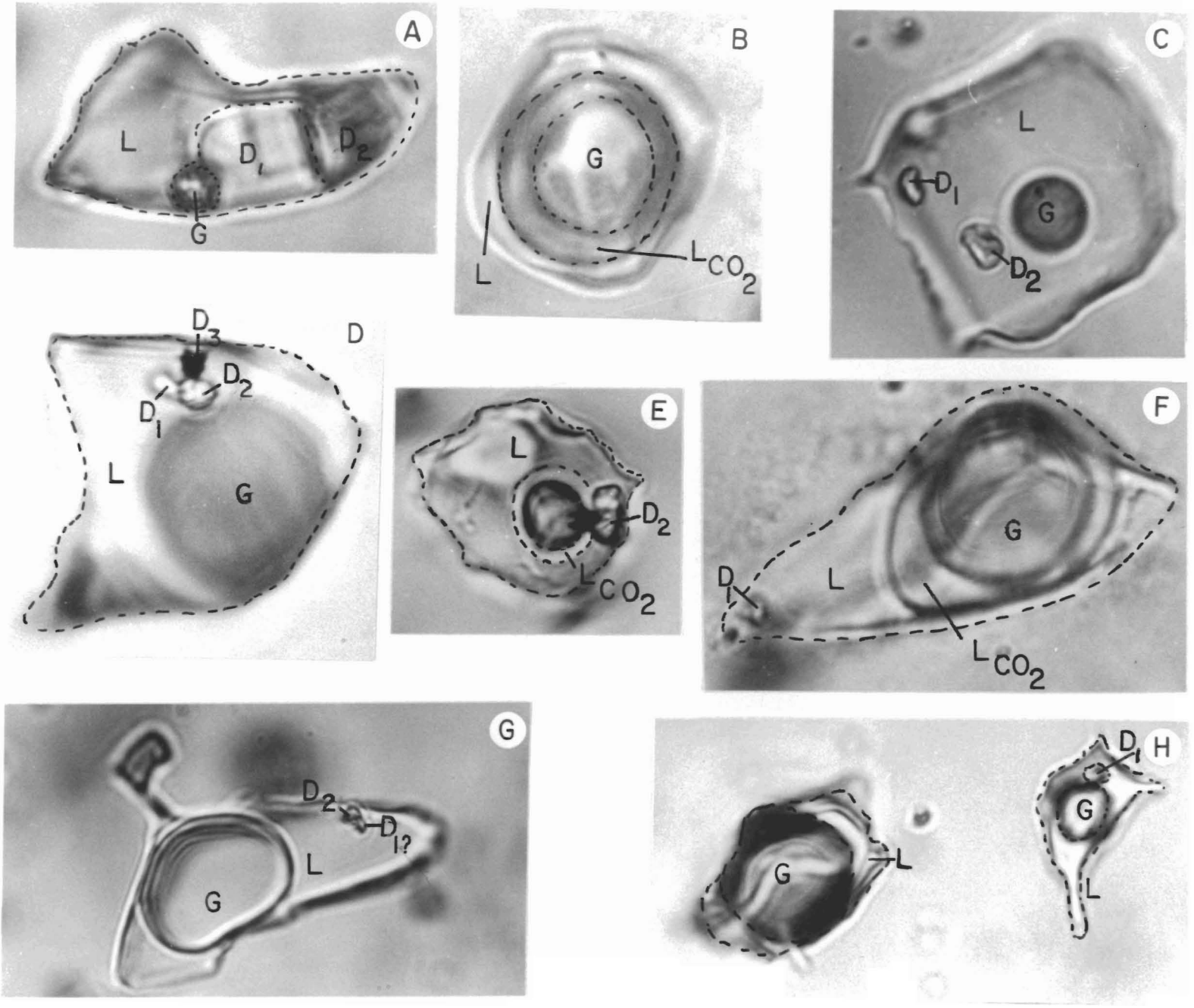
A
L
D1
D2
G
B
G
L
LCO2
C
L
D1
G
D2
D
D3
D2
D1
L
G
E
L
D2
LCO2
F
G
D1
L
LCO2
G
D2
D1?
L
G
H
G
L
D1
G
L

TABLE 8. Sulfur Isotope (δ^{34}) Values Relative to Meteoric Sulfur

The sample numbers refer to drill holes and depth shown in Figure 1A. The depths are in meters down from the collar of the drill hole. Numbers such as Pait, Moina 11, 12 refer to specific surface samples collected. The analyses were performed by Dr. Shen-Su-Sun, CSIRO Laboratories, North Ryde, N.S.W.

Drill hole and distance of sample down hole	Rock	Mineral	Value $\delta^{34}S$	Remarks
ML-1, 237 m	greisenized granite	pyrite	8.9	top of cupola is at 279 m
SMD 18, 102.50 m	metasomatized impure sandstone	pyrite	4.5	between wrigglite skarn and granite
Pait, Moina 11, 12	wrigglite	pyrite	8.8, 9.1	surface sample from near mill site, Shepherd and Murphy Mine
SMD 9, 102.50 m	pyrrhotite-rich skarn	pyrrhotite pyrite	8.6 8.4	pyrrhotite after magnetite wrigglite
SMD 14, 38 m	fine-grained dark dolomitic interbed in limestone	pyrrhotite	−4.1	above wrigglite, unaltered or metamorphosed
SMD 13, 93.50 m	sphalerite-rich skarn	sphalerite pyrite	9.3 8.4	sulfide-replaced wrigglite? on NE side of Bismuth fault
Surface sample	fine-grained dolomitic layer in limestone	pyrrotite pyrite	4.4 4.6	1.5 km from skarn
Pait, Moina 10	pyrite-rich skarn	pyrite	9.1	1.5 km from Moina skarn
Pait, Moina 7	framboidal pyrite, Moina sandstone	pyrite	−6.9	5 km from skarn

shapes which are not geometrically equivalent to folds in sedimentary bedding. The early stages of wrigglite skarn formation can clearly be demonstrated to be a replacement of preexisting limestone along fractures (Fig. 5C and D).

Superficially many wrigglite skarns appear to be a very selective specialized replacement of stromatolite layering (model 2). However, no stromatolites exist in the unreplaced carbonate host rocks known to the authors and in any case replacement demonstrably takes place outward from fractures, not specifically along a preexisting layering.

In model 3, limestone is progressively dissolved by acidic fluoride solutions and at the same time iron hydroxide and fluorite form as a gel precipitate, separating out by mutual attraction into separate layers as replacement proceeds. The gel crumples as replacement of the limestone proceeds irregularly, and the gel slowly ages to the present texture and mineralogy. Various similar processes have been proposed by Stevenson and Jeffery (1964), Boydell (1925) (quoted in Lovering, 1962), and Garrels and Dreyer (1952), for replacement of limestone by magnetite or sulfides. The model does explain the colloformlike texture of wrigglite skarn. However, Roedder (1968) demonstrated that colloformlike textures do not necessarily indicate that colloids have been present. Continuous layers in a gel when deformed would produce concentric folded shapes, not the reentrant angles commonly observed, and the volumetrically significant shrinkage cracks that occur in real gels are not observed in the lamination. If a gel intermediate stage existed on a large scale, the rock would have little strength and would be structurally unstable.

The model proposing that wrigglite skarns are crustiform precipitates in cavities (model 4) was first favored by Trustedt (1907). Presumably acid fluids infiltrate through limestone channels and produce fissurelike and pipelike openings. In the forward zone of the advancing front of fluids, the fluid passing by a given point is neutral to alkaline, and fluorite and magnetite (etc.) begin to precipitate. Slight fluctuations in the pH of the fluid cause the rhythmic layering until the cavity is filled or nearly filled. Crustiform layers necessarily build up from the walls of a cavity and are parallel to the walls. However, at Lost River and Moina, delicate argillaceous beds are preserved in wrigglite skarn whose layering is continuous on either side of the bed (Fig. 4C; and Sainsbury, 1969) suggesting that cavities could not have been present.

In model 5, fluids infiltrate along areas of high permeability while the components in the fluid replace and diffuse into the marble due to activity (and concentration) gradients. Wrigglite skarn forms by replacement at diffusion fronts advancing from the highly permeable area until the effective limiting distance of diffusion from the fracture is reached or until the fluid infiltrating along the fracture is spent. There are irregularities in the advancing diffusion fronts caused by slightly differing rates of diffusion from one place to another resulting in local thickening

and thinning. This produces the irregular fold forms in the wrigglite skarn. The last phase in the process is the filling of the fracture itself, to produce a coarser grained central vein of fluorite and other minerals, or further infiltration occurs producing alteration of wrigglite skarn by fluid(s) of different composition.

The mechanism to explain the rhythmic nature of the skarn is probably that discovered by Leisegang (quoted in Knopf, 1908). If a drop of $AgNO_3$ is placed upon a gelatin plate impregnated with $K_2Cr_2O_7$, a series of concentric rings of $Ag_2Cr_2O_7$ forms. These become progressively more widely spaced with increasing distance from the center, although the widening of the rings outward does not take place if the concentration at the center is kept constant by a continuous influx of material (Watanabe, 1924b). Five theories to explain the phenomenon and about 600 papers have been produced, as summarized by Stern (1954). Stern concluded that Ostwald's 1897 explanation is the most satisfactory. He believed that dichromate ions diffuse inward as Ag ions move outward. The continued diffusion caused super saturation of $Ag_2Cr_2O_7$ and precipitation at a front normal to the diffusion direction. Just beyond the front there is a zone of low concentration of dichromate and here Ag diffuses outward through this zone until it reaches inward-diffusing dichromate and supersaturation occurs once more, forming a new ring. The process can take place in solids and even in water (e.g., Leisegang, 1931; Stern, 1954). Watanabe (1924a) conducted experiments on the diffusion of mixed zinc and iron sulfate solutions through a sodium sulfide-impregnated gel. He produced alternating ZnS and FeS rhythmic layers. One boundary condition is that if the solution contains much Zn^{+2} and less Fe^{+2}, no rhythmic layering occurs, presumably because FeS can only precipitate when Zn^{+2} is exhausted at the leading edge. This rhythmic layering was found to be metastable, with the system eventually reverting to a granular structure. This may also be true of wrigglite skarns.

Beus (1966) and Eskola (1951) have attempted to explain the mechanism in exact terms. Beus believes that the leading front of the acidic solution is partly neutralized by reaction with carbonate and Fe oxide precipitates. The solution, now containing F-Al-Si-Be-Sn, etc., diffuses through this Fe oxide layer and a layer of fluorite plus other calc-silicate minerals precipitates. A new front of solution diffuses through this couplet, a new couplet forms, and so on. Beus's model is questionable because it does not explain the origin of wrigglite skarn in which no Fe oxide phase is present, such as some that occur at Lost River, Alaska. It also offers no adequate explanation for the fact that wrigglite skarn does not generally form in skarns poor in F, where granular skarn forms.

The mechanism proposed here is that extreme supersaturation of one component is necessary so that minerals containing that component (usually F) nucleate rapidly. Because of the extreme supersaturation of F in the carbonate environment, many small crystals of F minerals from the first layer. When this supersaturated component is depleted in the solution, other elements diffuse or perculate through the first formed layer to form the next wrigglite consisting of other minerals.

In the examples studied, when the thickness of successive couplets reaches a critical thickness of between 1 mm and 5 cm, fracturing and replacement of unreplaced marble occurs. At both Moina and at Mt. Garnet this critical thickness is greatest nearest the contact with the granite and least nearest the marble. Repeated periods of fracturing and vein filling explain the sequential nature of the vein contents shown in Figure 3. By sequential fracturing and replacement the entire marble unit is replaced (Fig. 4C) or if repeated fracturing does not occur, unreplaced marble is retained (Fig. 5C and D). The fracturing is interpreted to be in response to clogging of the system when the constituents of the solution can no longer diffuse across the distance to unreplaced marble and instead precipitate in the fracture system. The pressure needed to cause the fracturing may be caused by development of a CO_2 overpressure due to reactions occurring elsewhere in the skarn and, possibly, due to a tectonic component. This hypothesis best explains why fracturing is most intense within and peripheral to the skarn unit but not nearer the granite at Moina. The augen-type features containing granular skarn (Fig. 5C) are believed to represent the replacement of embayed marble where the conditions necessary for wrigglite skarn growth were not met (slow, systematic loss of CO_2?).

The rhythmic nature of the lamination could be caused by a constant supply of new solution passing through the fracture system as described by Watanabe (1924a). Alternatively, it could be caused by periodic opening and closing of the system at the end of each period of couplet formation. Spent CO_2-rich fluid would be flushed out of the system and wrigglite skarn formation would proceed from new introduced fluid. The periodic loss of volatiles (CO_2) may be essential for wrigglite skarn genesis because some skarns do contain much fluorine with Ca-Si silicates but do not have a wrigglite structure. This needs more study.

A model for the genesis of the skarn, quartz veins, and greisen at Moina

The assertion that the skarn, Sn-quartz veins, and greisen are cogenetic is supported by their close spatial relations and unique chemistry. As is shown by

the relict granite fabric and relict mineralogy in the greisen, fine-grained granite crystallized first. Its mineralogy was K-feldspar, plagioclase, quartz, F annite, and fluorite. The anomalous mica composition suggests the granite crystallized from a high f_{F_2} melt having high Fe/Fe + Mg and/or f_{O_2}, and relatively high SiO_2. The aqueous phase which evolved could not have been greatly out of equilibrium with the granite and some other process was needed to produce the greisenization.

When the pluton developed a solid granite carapace and dense surrounding hornfels, evolving aqueous solutions from lower levels were partly trapped. Rupturing of the carapace either by tectonic or fluid overpressure decreased P_{fluid} from values of $P_{lithologic}$ or more to values near $P_{hydrostatic}$. Boiling occurred producing an acidic, volatile-rich (HF, HCl, H_2S, etc.) vapor phase and a basic saline aqueous phase. As such, the system resembles a (small) porphyry copper system. The vapor phase caused greisenization of the granite and hornfels and facilitated the transport of much F and associated elements.

At Moina and many other wrigglite skarn deposits, massive granular skarns commonly occur between granite and wrigglite skarn (Govorov, 1958). The granular skarns consist mainly of garnet, vesuvianite, magnetite, pyroxene, and some fluorite. The garnet may be Sn rich (0.70 wt % at Moina to 0.3 at Iron Mountain, Jahns, 1944b) whereas vesuvianite commonly is Be bearing (to 1.30 wt % at Iron Mountain, Jahns, 1944b). Sn values in granular skarn are commonly high (e.g., in SMD 12, this study; at Iron Mountain, Jahns, 1944b), indicating that associated granular skarn is genetically related to the F-Sn-Be-bearing mineralization. However, this granular skarn has invariably been cut and partly altered by fluorine-adularia (-scheelite) veins (i.e., see Fig. 4B of this study for Moina; p. 80 of Sainsbury, 1969 for Lost River; p. 59 of Jahns, 1944b, for Iron Mountain). The veins are interpreted to have been the conduits for solutions which replaced marble to form wrigglite skarn higher in the sequence. The interpretation suggested here is that the granular skarn and hornfels were produced cogenetically with the granite and that the processes of greisenization, alteration of granular skarn, and formation of wrigglite skarn are associated with later boiling of the solutions.

The alteration of primary wrigglite and calc-silicate skarn by Zn-Cu-S-Cd-In-Au (group 2) precipitating solutions has been reported elsewhere (e.g., Aleksandrov, 1975) and occurs at Moina. At Moina, a zonal arrangement occurs on a regional scale with wolframite-cassiterite and accessory molybdenite nearest the Dolcoath granite; cassiterite with accessory wolframite and bismuthinite farther out; and Bi-Au and Ag-Pb-Au(-Zn) mineralization at the outer edge (Jennings, 1965, p. 513). A similar zonation associated with Sn-F skarn has been reported by Miroshnechenko and Gulyayev (1978, p. 54). The replacement of group 1 elements by group 2 metals occur outward from the Bismuth Creek fault. The alteration is interpreted to have occurred during the time when the system telescoped inward near the end of the mineralizing episode, superimposing base metal mineralization on group 1 mineralization. That primary (group 1) mineralization occurred by way of multiple fractures and faults (see Fig. 1A, magnetics), best explains the relatively even concentration of Sn, F, and Be in different drill holes. These fractures were eventually sealed by the precipitation of Sn-W-quartz veins.

The local alteration of the skarn to a hematite-quartz assemblage may have postdated the sulfide replacement as suggested by textural evidence (Fig. 5F). Whether the crystallization of type 2 mica, found associated with hematite in the greisen, is associated with hematite crystallization in skarn is not known. Presumably these minerals could have been produced when cooler, mainly meteoric water circulated through the system near the end of the mineralizing episode. Laumontite, which occurs in fractures in the skarn, may also relate to this episode, or may have formed later. The unreplaced limestone and siltstone above and peripheral to the skarn are of low metamorphic grade because they contain epidote + tremolite and calcite + quartz assemblages (Fig. 4E). The skarns, however, represent higher grade metamorphism as is indicated by the assemblage wollastonite + garnet + pyroxene. This, with the unique composition of all the skarns, suggests the skarn forms a pocket of high-grade metamorphism superimposed on a lower grade environment. The hydrothermal solutions may thus be the main source of the heat for the high-grade metamorphism and the heat was not produced from outward-moving isograds in response to conductive heat gained by the rocks from the cooling pluton.

Relation to other Sn-F replacement deposits

The relation between Sn-bearing wrigglite skarn deposits and massive Sn sulfide replacement deposits such as the Renison-Bell (Patterson, et al., 1981), Mt. Bischoff (Orr, 1976; Groves et al., 1972), and Cleveland (Palmer, 1976) deposits of Tasmania is unclear. These examples are replacements of both dolomite and limestone, and the mineralogy includes cassiterite, fluorite, and pyrrhotite. In each case extensive faulting occurred. However, magnetite-bearing wrigglite skarns occur near granite contacts (<250 m) and the other sulfide Sn-F deposits occur farther away (>500 ms?). Parts of the Mt. Bischoff and part of the

Moina deposits (Fig. 5E) appear to be transitional in having the assemblage pyrrhotite + fluorite + F-biotite ± cassiterite and also in being wrigglite.

Limited fluid inclusion data indicates that wrigglite skarns are at least partly produced from a boiling, high-temperature, saline solution whereas the non-wrigglite Sn replacement deposits are produced from nonboiling, lower temperature, and less saline solutions. The data of Collins (1979) suggest that for fluid inclusions studied from the Renison Bell and Cleveland deposits, homogenization temperatures range from 250° to 430°C, salinities are 10 to 15 weight percent (NaCl equivalent), and no evidence of boiling occurs. At Mt. Bischoff boiling appears to have occurred (Collins, 1979) with homogenization temperatures near 530° to 510°C and with fluid inclusions containing cubes of sylvite and halite (therefore, >26 equiv. wt % NaCl). Similar data has been produced in this study and in a study of the Mt. Garnet wrigglite skarns (study in progress by W. Brown and T. A. P. Kwak).

The relative importance of dolomites versus limestones as hosts is unclear because wrigglite skarn forms in dolomites (e.g., at Pitkaranta, USSR, Trustedt, 1907; at Chukotka, USSR, Getmanskaya, 1972; at Mt. Bischoff) as well as limestones.

Although more study is clearly needed, the above data can be used to imply that when suitable carbonate horizons exist near a "Sn"-leucogranite (<250 m) with the required plumbing system (i.e., faults), the result is the precipitation of a magnetite-cassiterite-fluorite wrigglite skarn from a boiling, high-temperature saline solution. However, if the carbonate horizon occurs at great distances from the pluton (>700 m) and the required permeability exists (such as the mineralized Bassett Federal fault at the Renison Bell deposit) and there is a source of sulfur, a massive cassiterite-pyrrhotite-fluorite-stannite replacement body forms from a lower temperature, nonboiling, more dilute solution. This has important economic consequences because only the latter type contains cassiterite in a form and quantity that is economically recoverable under present conditions.

Acknowledgments

Permission to publish this paper has been given by Comalco Limited. Discussions with D. M. Burt, A. Waite, and D. Veblen were very helpful. The Australian Research Grants Committee is thanked for giving access to electron microprobe facilities at the University of Melbourne and D. Sewell and P. Kelley of that institution are thanked for their help with the analyses. K. Palmer is thanked for help with the bulk chemical analyses. J. Hannah of the University of California, Davis, is thanked for help with computational problems and last, but certainly not least, B. Taylor of the same institution is thanked both for much helpful discussion and for supplying some mineral analyses.

May 15, 1979; September 8, 1980

REFERENCES

Aleksandrov, S. M., 1975, The geochemistry of formation of skarns and ores in the crushed zones of carbonate rocks: Geochemistry Internat., v. 12, no. 5, p. 2–18.

AMDEL, 1978, Report on the distribution of tin in ores from Moina, Tasmania: Adelaide, AMDEL, Rept. R 745, 6 p.

Askins, P. W., 1975, "Wrigglite"—an unusual fluorite bearing skarn, Mt. Garnet region, North Queensland, Australia: Unpub. M.Sc. thesis, Cairns, Australia, James Cook Univ., 185 p.

—— 1978, "Wrigglite"—a fluorite rich skarn at Moina, Tasmania, and The Shepherd and Murphy Mine, *in* Geology and mineralization of N. W. Tasmania: Hobart, Geol. Soc. Australia Spec. Pub. p. 9–10.

Beus, A. A., 1966, Geochemistry of beryllium and genetic types of beryllium deposits: San Francisco, W. H. Freeman and Co., 401 p.

Boydell, H. C., 1925, The role of colloidal solutions in the formation of mineral deposits: Inst. Mining Metallurgy Trans., v. 34, sec. B, p. 145–337.

Collins, P. L. F., 1979, Fluid inclusions in cassiterite-sulphide metasomatic replacement deposits, *in* Kwak, T. A. P., ed., Fluid inclusion workshop notes, Study Group for Economic Geology, La Trobe University, Feb. 26–29: Melbourne, Geol. Soc. Australia, 85 p.

Ermilova, L. P., and Senderova, U. M., 1959, Strontianite from the West Kara-Ob deposit in central Kazakhstan: Materialy po geologii rudnykh mesotorozhdenii, petrografii mineralogii i geokhimii, Izdatel-stvo AN SST, p. 294–300.

Eskola, P., 1951, Around Pitkaranta: Soumalaisen Tiedeakatemian Toimituksia (Annales), ser. A., v. 3, no. 27, 90 p.

Garrels, R. M., and Dreyer, R. M., 1952, Mechanism of limestone replacement at low temperatures and pressures: Geol. Soc. America Bull., v. 63, p. 325–380.

Gee, C. E., 1966, The geology and mineral deposits of the Moina-Lorinna area: Unpub. B.Sc. Honours thesis, Univ. Tasmania, 132 p.

Georgievskaya, O. G., 1955, Genesis of the rhythmic-folded laminated texture of ore bodies of some contact-metasomatic deposits (K. vopruso o genezise vitmichno-vitievato-potoschatoi tekstury vudnykh tel nekotorhykh kontakto-metasomatischeskikh mestoroschdeneii) Akad. Nauk SSSR Doklady, v. 101, no. 5, p. 87–96.

Getmanskaya, T. I., 1972, Beryllium mineralization in a polymetallic ore district in Siberia: Internat. Geol. Rev., v. 14, p. 829–836.

Green, D. C., 1979, Moina "wrigglite": Tasmania Dept. Mines, unpub. rept. R.758, R.745, R.731, 5 p.

Govorov, M. M., 1968, Specific features of mineralogy and genesis of tin-beryllium-fluorite deposits of the Far East: Akad. Nauk SSSR Izv., Ser. Geol., no. 1, p. 62–73.

Groves, D. I., Martin, E. L., Mruchies, H., and Wellington, H. K., 1972, A century of tin mining at Mount Bischoff, 1871–1971: Tasmania Dept. Mines Geol. Survey Bull. 54, p. 3–10.

Holser, W. T., and Kaplan, I. R., 1966, Isotope geochemistry of sedimentary sulfates: Chem. Geology, v. 1, p. 93–135.

Hsieh, C. Y., 1963, A study of tin deposits in China: Scientia Sinica, v. 12, p. 373–390.

Jahns, R. H., 1944a, "Ribbon Rock," an unusual beryllium-bearing tactite: Econ. Geol., v. 39, p. 173–205.

—— 1944b, Beryllium and tungsten deposits of the Iron Mountains

district, Sierra and Socorro Counties, New Mexico: U. S. Geol. Survey, Bull. 945-L, 79 p.

Jennings, I. B., 1963, Middlesex, one mile geological series, explanatory report: Tasmania Geol. Survey, Expl. Rept., p. 512–514.

Jennings, I. B., 1965, Middlesex mineral district, *in* McAndrew, J., ed., Geology of Australian ore deposits: Melbourne, Australasian Inst. Mining Metallurgy, v. 1, p. 512–514.

Knopf, A., 1908, Geology of the Seward Penninsula tin deposits, Alaska: U. S. Geol. Survey Bull. 358, 71 p.

Leisegang, R. E., 1931, Colloid chemistry and geology, *in* Alexander, J., ed., Colloid chemistry, vol. 3: Cambridge, Chem. Category Co., 187 p.

Lovering, T. G., 1962, The origin of jasperoid in limestone: ECON. GEOL., v. 62, p. 861–889.

Mason, P. K., Frost, M. T., and Read, S. J. B., 1969, Computor programs for calculating corrections in quantitative X-ray mind-analysis: United Kingdom, Nat. Physics Lab., Div. Inorganic Metallic Structure, rept. 2, 45 p.

Meng, H. H., 1937, Tin deposits of China: Geol. Soc. China, Bull. 17, p. 439–449.

Miroshnchenko, L. A., and Gulyayev, A. P., 1978, Skarn-greisen metasomatism: Alma-Ata Nauka, Kazakstan SSR, 167 p.

Miyake, H., 1965, Study on genesis on skarns and the related minerals: Hiroshima Univ. Jour. Sci., ser. C., v. 4, p. 37–49.

Norrish, K., and Hutton, J. T., 1969, An accurate X-ray spectrographic method for the analysis of a wide range of geological samples: Geochim. et Cosmochim. Acta, v. 33, p. 431–453.

Ohmoto, H., and Rye, R. O., 1979, Isotopes of sulfur and carbon, *in* Barnes, H. L., ed., Geochemistry of hydrothermal ore deposits, 2nd ed.: New York, Wiley-Interscience, p. 509–567.

Orr, D., 1976, The Mt. Bischoff tin deposit: Internat. Geol. Cong., 25th, Sydney 1976, Excursion Guide 31AC, p. 19–23.

Palmer, K. C., 1976, The Cleveland tin deposit: Internat. Geol. Cong. 25th, Sydney 1976, Excursion Guide 31AC, p. 27–31.

Patterson, D. J., 1976, The Renison tin deposit: Internat. Geol. Cong., 25th, Sydney 1976, Excursion Guide 31AC, p. 37–39.

Perry, D. 1964, Genesis of the contact rocks at the Abril mine, Cochise Country, Arizona: Unpub. M.Sc. thesis, Univ. Arizona, 156 p.

Reid, K. O., 1971, Moina area: Queenstown, Mt. Lyell Mining Railway Co. Internal. memorandum E. L. 8/65, 52 p.

Roedder, E., 1968, The non-collodial origin of "colloform" textures in sphalerite ores: ECON. GEOL., v. 63, p. 451–471.

Sainsbury, C. L., 1964, Geology of the Lost River mine area, Alaska: U. S. Geol. Survey Bull. 1129, 80 p.

—— 1969, Geology and ore deposits of the central York Mountains, western Seward Peninsula, Alaska: U. S. Geol. Survey Bull. 1287, 69 p.

Shabynin, L. I., 1977, The origin of rhythmically banded skarn-greisen structures: Geokhimiya, no. 9, p. 1424–1435.

Shcherba, G. N., 1970, Greisens; Internat. Geol. Rev., v. 12, p. 114–150, 239–255.

Shima, M., Gross, W. H., and Thode, H. G., 1963, Sulfur isotope abundances in basic sills, differentiated granites and meteorites: Jour. Geophys. Research, v. 68, p. 2835–2846.

Stern, K. H., 1954, The Liesegang phenomenon: Chem. Rev., v. 54 (1), p. 79–99.

Stevenson, J. S., and Jeffery, W. G., 1964, Colloform magnetite in a contact metasomatic iron deposit, Vancouver Island, British Columbia: ECON. GEOL., v. 59, p. 1298–1305.

Trustedt, O., 1907, Die Erzlagerstatten von Piktaranta am Ladoga: Comm. Geol. Finlande Bull., no. 19, 57 p.

Twelvetrees, W. H., 1913, The Middlesex and Mt. Claude mining field: Tasmania Geol. Survey Bull. 14, 28 p.

Waite, A., 1978, The petrology, mineralogy and genesis of the tin-fluorine-tungsten skarn of Moina, Tasmania: Unpub. B.Sc. Honours thesis, Bundoora, Australia, La Trobe Univ., 57 p.

Watanabe, M., 1924a, Zonal precipitation of ores from a mixed solution: ECON. GEOL., v. 19, p. 497–503.

—— 1924b, Some problems of diffusion, with special reference to study of ore deposits: Tohoku Imp. Univ. Sci. rept., ser. 3., v. 3, p. 105–189.

Williams, K. L., 1958, Tin-tungsten mineralization at Moina, Tasmania: Australasian Inst. Mining Metallurgy, Proc., no. 185, p. 29–50.

Zasedatelev, A. M., 1973, The problem of genesis of berylliferous skarns: Internat. Geol. Rev., v. 15, p. 213–224.